[redacted]

ORNL-2189
Progress Cy. 90-A
C-84 – Reactors–Special Features of Aircraft Reactors

AEC RESEARCH AND DEVELOPMENT REPORT

CENTRAL RESEARCH LIBRARY
DOCUMENT COLLECTION

MARTIN MARIETTA ENERGY SYSTEMS LIBRARIES
3 4456 0350335 9

DECLASSIFIED
CLASSIFICATION CHANGED TO:
BY AUTHORITY OF: AEC - 7-12-60
BY: [illegible] 8/16/68

SOLID STATE DIVISION

SEMIANNUAL PROGRESS REPORT

FOR PERIOD ENDING AUGUST 30, 1956

CENTRAL RESEARCH LIBRARY
DOCUMENT COLLECTION
LIBRARY LOAN COPY
DO NOT TRANSFER TO ANOTHER PERSON
If you wish someone else to see this document, send in name with document and the library will arrange a loan.

OAK RIDGE NATIONAL LABORATORY
OPERATED BY
UNION CARBIDE NUCLEAR COMPANY
A Division of Union Carbide and Carbon Corporation
UCC
POST OFFICE BOX X · OAK RIDGE, TENNESSEE

[redacted]

LEGAL NOTICE

This report was prepared as an account of Government sponsored work. Neither the United States, nor the Commission, nor any person acting on behalf of the Commission:

A. Makes any warranty or representation, express or implied, with respect to the accuracy, completeness, or usefulness of the information contained in this report, or that the use of any information, apparatus, method, or process disclosed in this report may not infringe privately owned rights; or

B. Assumes any liabilities with respect to the use of, or for damages resulting from the use of any information, apparatus, method, or process disclosed in this report.

As used in the above, "person acting on behalf of the Commission" includes any employee or contractor of the Commission to the extent that such employee or contractor prepares, handles or distributes, or provides access to, any information pursuant to his employment or contract with the Commission.

[redacted]

ORNL-2189
Progress
C-84 – Reactors–Special Features of Aircraft Reactors

This document consists of 46 pages.

Copy 90 of 213 copies. Series A.

Contract No. W-7405-eng-26

SOLID STATE DIVISION

SEMIANNUAL PROGRESS REPORT

For Period Ending August 30, 1956

D. S. Billington, Director
J. H. Crawford, Jr., Assistant Director

DATE ISSUED

NOV 28 1956

OAK RIDGE NATIONAL LABORATORY
Operated by
UNION CARBIDE NUCLEAR COMPANY
A Division of Union Carbide and Carbon Corporation
Post Office Box X
Oak Ridge, Tennessee

[redacted]

MARTIN MARIETTA ENERGY SYSTEMS LIBRARIES

3 4456 0350335 9

[redacted]

Reports previously issued in this series are:

ORNL-1025	Period Ending January 31, 1951
ORNL-1095	Period Ending April 30, 1951
ORNL-1128	Period Ending July 31, 1951
ORNL-1214	Period Ending October 31, 1951
ORNL-1261	Period Ending January 31, 1952
ORNL-1301	Period Ending May 10, 1952
ORNL-1359	Period Ending August 10, 1952
ORNL-1429	Period Ending November 10, 1952
ORNL-1506	Period Ending February 10, 1953
ORNL-1606	Period Ending August 31, 1953
ORNL-1677	Period Ending February 28, 1954
ORNL-1762	Period Ending August 30, 1954
ORNL-1861	Period Ending February 28, 1955
ORNL-1944	Period Ending August 30, 1955
ORNL-1945	Period Ending August 30, 1955
ORNL-2051	Period Ending February 29, 1956
ORNL-2052	Period Ending February 29, 1956

[redacted]

[redacted]

[redacted]

ORNL-2189
Progress
C-84 – Reactors–Special Features of Aircraft Reactors

INTERNAL DISTRIBUTION

1. C. D. Baumann
2. [redacted] G. Berggren
3. J. [redacted]. Betterton, Jr.
4. D. S. Billington
5. D. Bi[redacted]er
6. T. H. B[redacted]witt
7. A. L. Bo[redacted]
8. C. D. Bopp
9. G. E. Boyd
10. H. Brooks (con[redacted]ltant)
11. W. E. Browning
12. W. E. Brundage
13. D. W. Cardwell
14. R. M. Carroll
15. C. E. Center
16. R. A. Charpie
17. J. W. Cleland
18. A. F. Cohen
19. D. D. Cowen
20. J. H. Crawford, Jr.
21. F. L. Culler
22. J. E. Cunningham
23. R. R. Dickison
24. S. E. Dismuk[redacted]
25. L. B. Emlet (K-25)
26. J. H. Fry[redacted], Jr.
27. J. L. G[redacted]bbard
28. R. J. [redacted]ray
29. W. O. [redacted]Harms (consultant)
30. C. S. Harrill
31. A. [redacted]Hollaender
32. [redacted]. K. Holmes
33. A. S. Householder
34. J. T. Howe
35. H. B. Huntington (consultant)
36. L. K. Jetter
37. R. W. Johnson
38. R. J. Jones
39. W. H. Jordan
40. G. W. Keilholtz
41. C. P. Keim
42. M. T. Kelley
43. R. H. Kernohan
44. E. M. King
45. H. V. Klaus
46. J. A. Krumhansl (consultant)
47. T. A. Lincoln
48. S. C. Lind
49. R. S. Livingston
50. H. G. MacPherson
51. W. D. Manly
52. C. J. McHargue
53. A. J. Miller
54. E. C. Miller
55. J. G. Morgan
56. K. Z. Morgan
57. M. T. Morgan
58. E. J. Murphy
59. J. P. Murray (Y-12)
60. M. L. Nelson
61. T. S. Noggle
62. R. B. Oliver
63. P. M. Reyling
64. A. E. Richt
65. M. T. Robinson
66. E. S. Schwartz
67. H. C. Schweinler
68. F. Seitz (consultant)
69. E. D. Shipley
70. O. Sisman
71. M. J. Skinner
72. G. P. Smith
73. A. H. Snell
74. R. L. Sproull (consultant)
75. E. E. Stansbury
76. D. K. Stevens
77. C. D. Susano
78. [redacted] A. Swartout
79. [redacted] H. Taylor
80. M. [redacted]. Wechsler
81. R. [redacted] Weeks
82. A. M. [redacted]Weinberg
83. E. P. [redacted]igner (consultant)
84. G. C. Williams
85. J. C. Wilson
86. C. E. Winters

[redacted]

[redacted]

87. M. C. Wittels
88. Biology Library
89–91. Central Research Library
92. Health Physics Library
93–97. Laboratory Records Department
98. Laboratory Records, ORNL R.C.
99. ORNL – Y-12 Technical Library, Document Reference Section
100. Reactor Experimental Engineering Library

EXTERNAL DISTRIBUTION

101. AF Plant Representative, Baltimore
102. AF Plant Representative, Burbank
103. AF Plant Representative, Marietta
104–106. AF Plant Representative, Santa Monica
107–108. AF Plant Representative, Seattle
109. AF Plant Representative, Wood-Ridge
110. Air Materiel Area
111. Air Research and Development Command (RDGN)
112. Air Technical Intelligence Center
113. Allison Division
114–116. ANP Project Office, Fort Worth
117. Albuquerque Operations Office
118. Argonne National Laboratory
119. Armed Forces Special Weapons Project, Sandia
120. Armed Forces Special Weapons Project, Washington
121. Assistant Secretary of the Air Force, R&D
122–127. Atomic Energy Commission, Washington
128. Battelle Memorial Institute
129–130. Bettis Plant (WAPD)
131. Bureau of Aeronautics
132. Bureau of Aeronautics (Code 24)
133. Bureau of Aeronautics General Representative
134. Chicago Operations Office
135. Chicago Patent Group
136. Chief of Naval Research
137. Convair-General Dynamics Corporation
138. Engineer Research and Development Laboratories
139–143. General Electric Company (ANPD)
143. Hartford Area Office
144. Headquarters, Air Force Special Weapons Center
145. Idaho Operations Office
146. Knolls Atomic Power Laboratory
147. Lockheed Aircraft Corporation (R. G. Rowe)
148. Lockland Area Office
149. Los Alamos Scientific Laboratory
150. National Advisory Committee for Aeronautics, Cleveland
151. National Advisory Committee for Aeronautics, Washington
152. Naval Air Development and Material Center
153. Naval Research Laboratory
154. New York Operations Office
155. North American Aviation, Inc. (Aerophysics Division)

[redacted]

[redacted]

156. North American Aviation, Inc. (Canoga Park)
157. Nuclear Development Corporation of America
158. Office of the Chief of Naval Operations (OP-361)
159. Patent Branch, Washington
160–163. Pratt and Whitney Aircraft Division (Fox Project)
164. Sandia Corporation
165. School of Aviation Medicine
166. Sylvania Electric Products, Inc.
167. USAF Project RAND
168. University of California Radiation Laboratory, Livermore
169–186. Wright Air Development Center (WCOSI-3)
187–211. Technical Information Service Extension, Oak Ridge
212. Division of Research and Development, AEC, ORO
213. Technical Research Group, New York

[redacted]

[redacted]

CONTENTS

SUMMARY 1

ANP RADIATION DAMAGE 3

- Examination of Disassembled MTR In-Pile Loops 3, 4, and 5 3
- Investigation of Materials Removed from MTR In-Pile Loops 3 and 5 9
- Effect of Radiation on Static Corrosion of Structural Materials by Fused Salt Fuels 10
- LITR Vertical In-Pile Loop 11
- ART Off-Gas System Instrumentation Analysis 15
- Design Calculations for the Vertical Miniature In-Pile Loop 15
- ART Reactivity Transients Associated with Fluctuations in Xenon-Removal Efficiency 20
- Use of Zr^{95} as a Fission Monitor 23

HOT METALLOGRAPHY 24

HOT-CELL OPERATION 25

RADIATION METALLURGY 26

- Creep and Stress-Corrosion Tests of Inconel 26
- MTR Stress-Corrosion Apparatus 26
- Irradiation of Shielding Materials 26

ENGINEERING PROPERTIES 28

- High-Temperature Ceramic Fuels 28
  - Fuel Irradiations 28
  - Autoradiography of Fuel Plates 28
  - Fission-Gas Release 31
- Reactor Shield Materials 32
  - Boron Carbide 34
  - MTR Irradiations 35
  - Boron Nitride 37

[redacted]

[redacted]

[redacted]

[redacted]

SOLID STATE DIVISION SEMIANNUAL PROGRESS REPORT

SUMMARY

ANP RADIATION DAMAGE

MTR in-pile loop 3 has been disassembled, and all components except the pump impeller have been examined metallographically. Loop 5, which could not be filled, has been disassembled. No evidence of a mechanical or metallic plug was found in the fuel system. Fuel samples were obtained from various sections of the fuel system for chemical analysis.

Chemical analyses of samples from MTR loop 3 indicated that the amber material from the pump was probably an oil decomposition product. Considerable amounts of Cs^{137} and Sr^{89} were found in the off-gas line and less abundantly in the fission-gas-adsorber trap. Iron, chromium, and nickel analyses of the fuel confirmed that little corrosion had occurred.

Irradiation of static corrosion capsules in the MTR has been continued. Two Inconel capsules containing the fuel mixture $NaF\text{-}ZrF_4\text{-}UF_4$ were irradiated at 6 kw/cm^3 for over nine weeks. One of them leaked fission activity after a temperature excursion, but contamination control by freezing the fuel made reactor power interruption unnecessary. Two other capsules are being irradiated at 6 kw/cm^3. Preparation of Hastelloy B capsules containing an $NaF\text{-}KF\text{-}LiF\text{-}UF_4$ fuel mixture continued. The present design of the MTR fused salt capsule facility is illustrated.

The cause of pump failure in the LITR vertical in-pile loop was found to be a loose shear pin which had lodged in the impeller, throwing it out of balance and bending the shaft until it rubbed against the impeller housing. Future internal loop parts will be fastened by welding. Thermal mockup and bearing tests have been run on a modified shaft which is shorter and stiffer and which has better bearings. Pump performance tests were run with water to optimize impeller clearances, and the results were interpreted in terms of fuel Reynolds number in the loop using the optimized pump. A full-scale bench test pump is being assembled, and in-pile loop parts are being modified to conform with the improved pump design.

Tests are being prepared for determining the effect of the unusual geometry on resolution, sensitivity, and general performance of scintillation gamma-ray spectrometers of the type to be used on the ART off-gas system.

A new electronic analog circuit has been developed for simulation of the thermal behavior of the vertical miniature in-pile fuel loop. A series of calculations has been made which illustrates the behavior of the loop when circulating fluoride fuel composition 41 in position C-46 of the LITR.

Electronic analog simulation has been used to investigate the possibility that fluctuations in the efficiency of removal of xenon from the fuel by the pumps might cause troublesome reactivity transients. It was found that no transient of a period short enough to cause concern for the controllability of the ART exists.

The fission yield of 65-day Zr^{95} has been determined in enriched U_3O_8 and in fluoride fuel composition 44 by comparison with the yield of 33-year Cs^{137}. For use in fission monitoring, the yield found for Zr^{95} is 0.0664 ± 0.0013 atom/fission.

HOT METALLOGRAPHY

Metallographic examinations of components, coupons, and stress-corrosion specimens submitted by HRP personnel and of portions of components from the North Carolina State College Reactor have been completed, and the results have been reported elsewhere. Examination of two additional in-pile loops is now in progress, and sections and specimens from two additional loops are awaiting examination.

Postirradiation examination of specimens from the APPR Program has been initiated. Approximately one half of the 26 small-size fuel plates have been examined. Some sections from a full-size fuel element have also been examined. Work is continuing on both phases of this program.

Examination of the ANP in-pile loop 3 has been completed, and a final report will be issued soon. MTR in-pile loop 5 was disassembled in an attempt to determine the reason why the loop could not be filled when it was inserted in the MTR. No evidence of a mechanical or metallic plug was found which would account for such a failure. However, the fill line contained a substance of an

[redacted]

extremely different physical appearance from that of the normal fuel mixture, and samples were obtained for chemical analysis. Disassembly of in-pile loop 4 is now in progress.

HOT-CELL OPERATIONS

ANP in-pile loop 5 and another LITR vertical in-pile loop were disassembled and then examined in the hot cells. The disassembly of ANP in-pile loop 4 was started. The new analytical balance was placed into remote operation. The cell-use data for the first six months of 1956 did not differ appreciably from those for 1955.

RADIATION METALLURGY

The time to rupture of internally stressed, thin-walled Inconel tubes was found to be reduced by irradiation at 1500°F in the LITR.

Creep and compression tests on copper–boron carbide compacts have been operated at elevated temperatures. High-temperature deformation was found to strengthen the material.

ENGINEERING PROPERTIES

High-Temperature Ceramic Fuels

Static irradiations were completed on four SiC-Si-UO_2 fuel plates containing 4 wt % UO_2. The plates were thermally cycled many times, and maximum temperatures of 1740°F were obtained by self-fission heating. Postirradiation examinations of property changes have been started. The samples remained dimensionally stable. Samples of ThO_2-UO_2 containing 2½% UO_2 were irradiated to a total thermal-neutron dosage of up to 1×10^{20} *nvt* and at temperatures up to 1925°F. These samples also remained dimensionally stable.

A method was developed for making autoradiograph pictures of the irradiated fuel plates by use of a lead pinhole camera. The location of the fission products in the core of the plate was determined and was compared with x-ray photographs of the plate before irradiation.

High-Temperature Shield Materials

The results of the irradiation survey of several boron carbide bodies are reported. With one exception, samples retained favorable bulk properties when they were irradiated to a thermal-neutron dosage of up to 6×10^{19} *nvt*. Boron nitride powder samples were obtained and analyzed. Irradiations are planned on pressed bodies of this material.

Metallographic data were obtained on a stainless-steel-clad CaB_6-Fe sample that had been irradiated in the LITR. Additional samples were inserted for further irradiations. Irradiation tests were started on a stainless-steel-clad boron-nitride–nickel cermet. One exposure is being carried out at room temperature in a water-cooled facility in the LITR; the other exposure is being carried out in a high-temperature facility, which maintains the sample at 1600°F in a vacuum.

An experiment was developed and shipped to the MTR for the irradiation of neutron shield materials at elevated temperatures. The first material to be tested is a stainless-steel-clad copper–boron carbide cermet. The planned temperature of irradiation is 1600°F.

ANP RADIATION DAMAGE

G. W. Keilholtz

EXAMINATION OF DISASSEMBLED MTR IN-PILE LOOPS 3, 4, AND 5

A. E. Richt
E. J. Manthos C. Ellis
W. B. Parsley R. M. Wallace
E. D. Sims R. N. Ramsey

Examination of loop 3 has been completed except for metallographic examination of the pump impeller. Corrosion of the nose coil varied from 1 mil near the inlet side to a maximum of 3 mils of intergranular attack near the outlet side (Fig. 1). Comparisons of the inner wall of the nose-coil tubing on the compression side of the coil with the opposite inner wall on the tension side showed no differences in the depth of attack. The depths of attack found on the straight sections of the fuel tube are compared in Fig. 2. Figures 3 through 8 show the attack found on specimens from various points in the loop. No mass-transferred crystals were found on any of the specimens.

Disassembly of loop 4 has begun, but as yet no results are available.

Loop 5, which was inserted in the MTR but could not be filled, was shipped to ORNL for disassembly after the section behind the pump motor was removed at the MTR. Several other operating difficulties encountered during the attempt to fill the loop were chattering of the fuel-circulating pump, improper functioning of some of the thermocouples, leakage occurring through the pump bulkhead, and failure of a fill-line Calrod heater after it had been raised to higher than normal operating temperatures.

Fuel was found in the nose inlet fuel line 24 1/2 in. from the face, and a shallow layer of fuel was found in the outlet line from the nose coil at the same distance from the pump. The fuel in the inlet and outlet lines at a point 22 3/4 in. from the face of the pump is shown in Fig. 9.

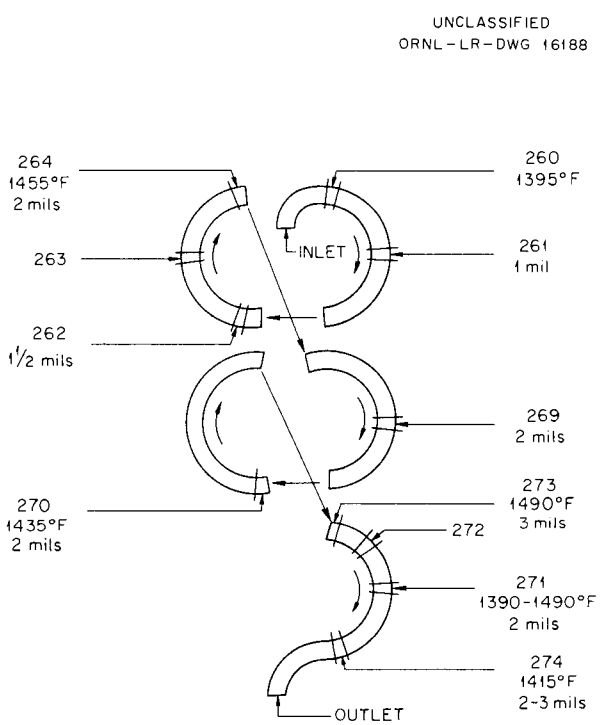

Fig. 1. Diagram of Sectioned Nose Coil of MTR In-Pile Loop 3 Showing Locations from Which Metallographic Samples Were Taken, the Maximum Temperature Which Occurred at the Particular Location During Operation, and the Depth of Corrosive Attack Found by Subsequent Metallographic Examination of the Samples.

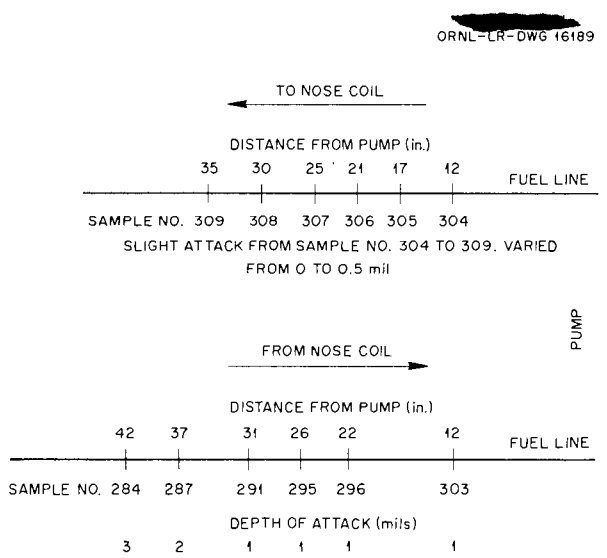

Fig. 2. Comparison of Depths of Attack on Straight Sections of Fuel Tubing from In-Pile Loop 3.

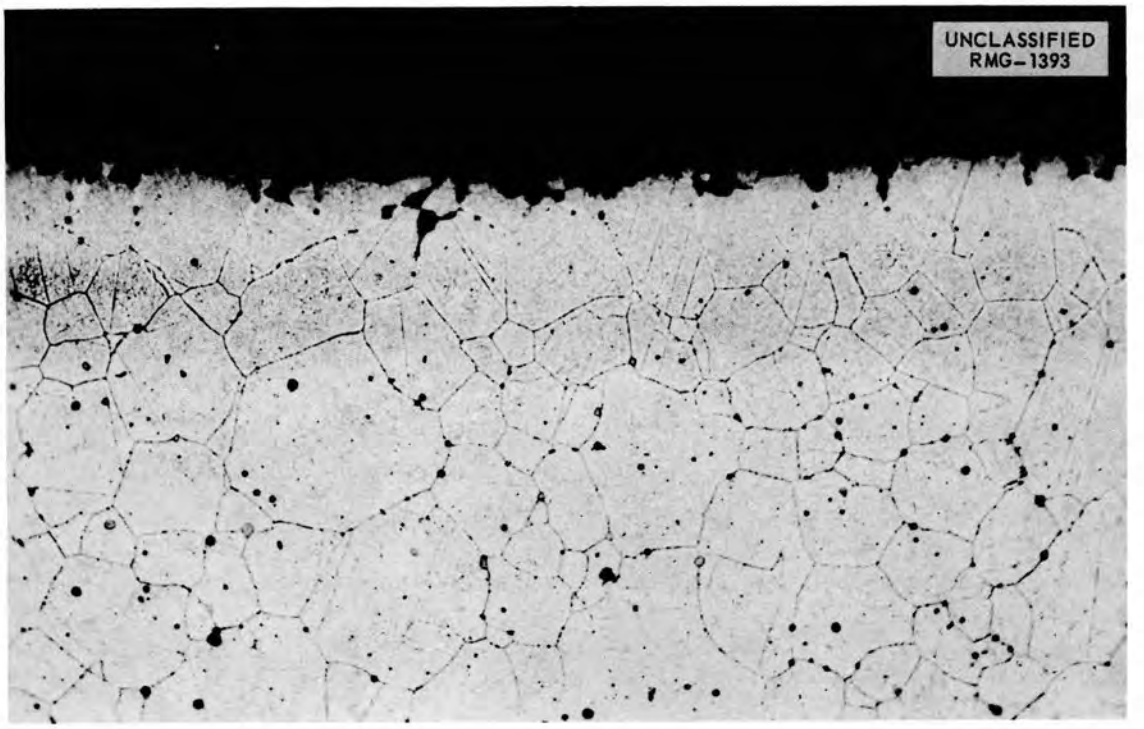

Fig. 3. Sample No. 264, Taken Near Inlet End of Nose Coil of MTR In-Pile Loop 3, Showing Intergranular Corrosion to a Depth of 2 mils. 250X. (Confidential with caption)

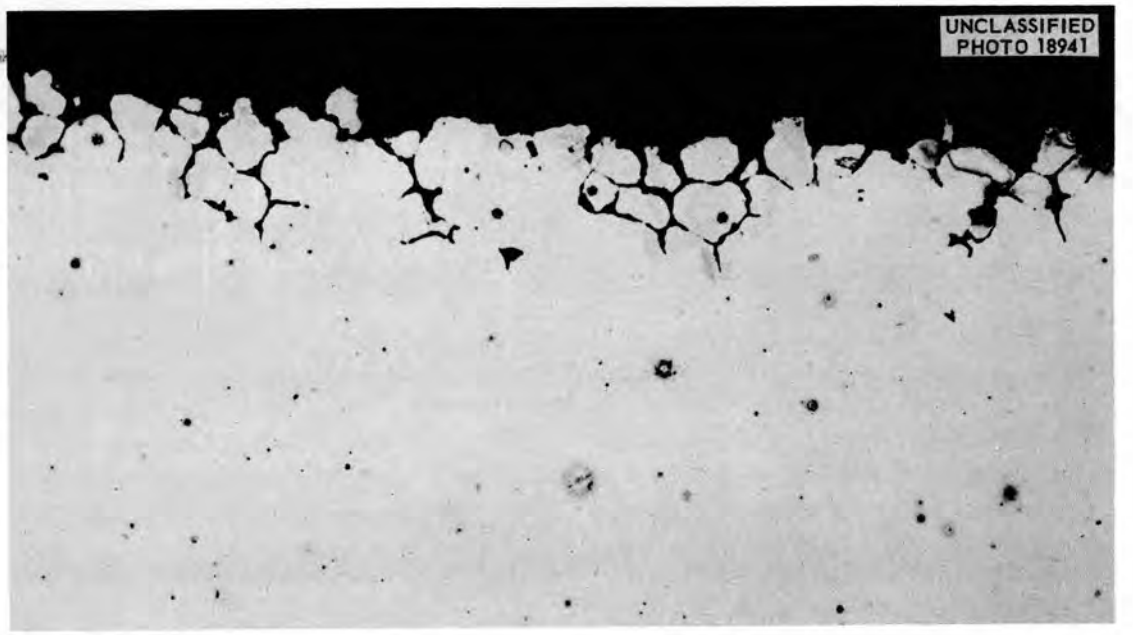

Fig. 4. Sample No. 273, Taken Near Outlet End of Nose Coil of MTR In-Pile Loop 3, Showing Intergranular Corrosion to a Depth of 3 mils. Sample lightly etched. 250X. (Confidential with caption)

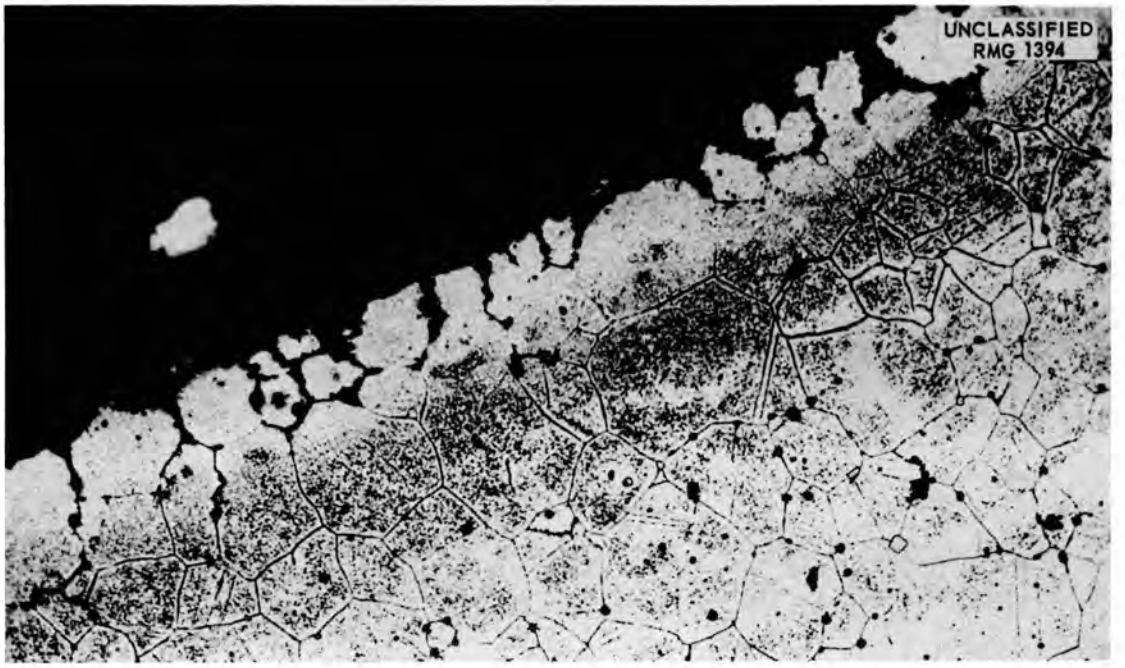

Fig. 5. Sample No. 273, Given a Deeper Etch Than in Fig. 4. 250X.

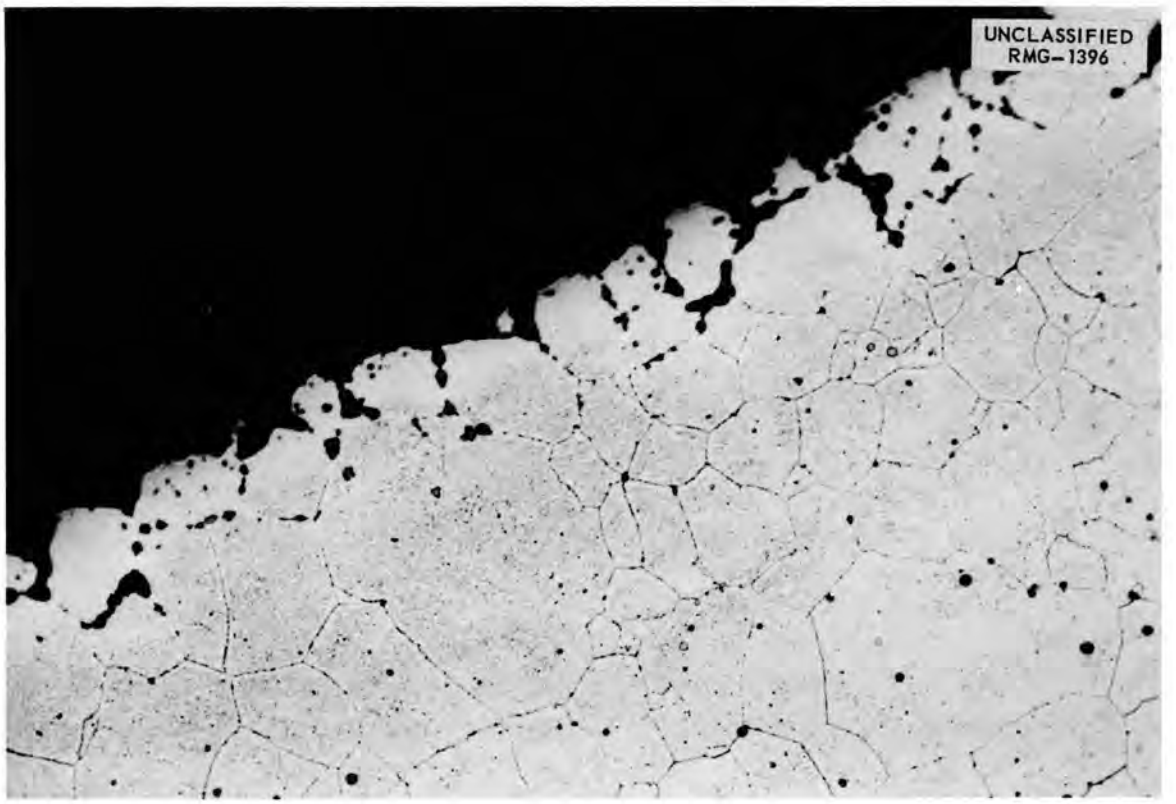

Fig. 6. Sample No. 284, Taken from Straight Section of Fuel Tubing Near Outlet of Nose Coil at a Point 42 in. from the Pump of MTR In-Pile Loop 3. Intergranular corrosion to a depth of 3 mils can be seen. 250X. (Confidential with caption)

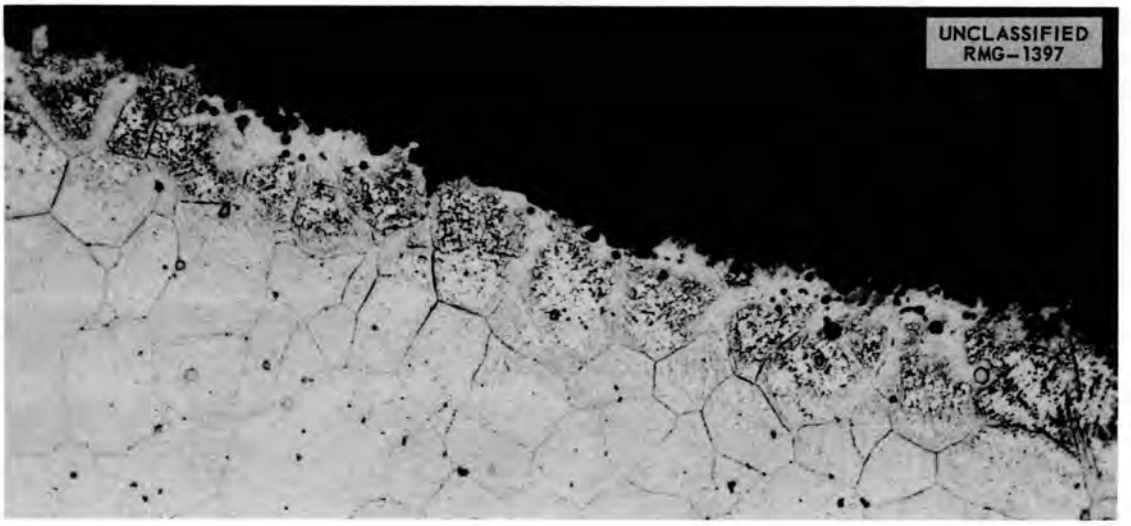

Fig. 7. Sample No. 303, Taken from Straight Section of Fuel Tubing Between the Nose Coil Outlet and the Pump at a Point 12 in. from the Pump of MTR In-Pile Loop 3. Intergranular corrosion to a depth of 1 mil can be seen. 250X. (Confidential with caption)

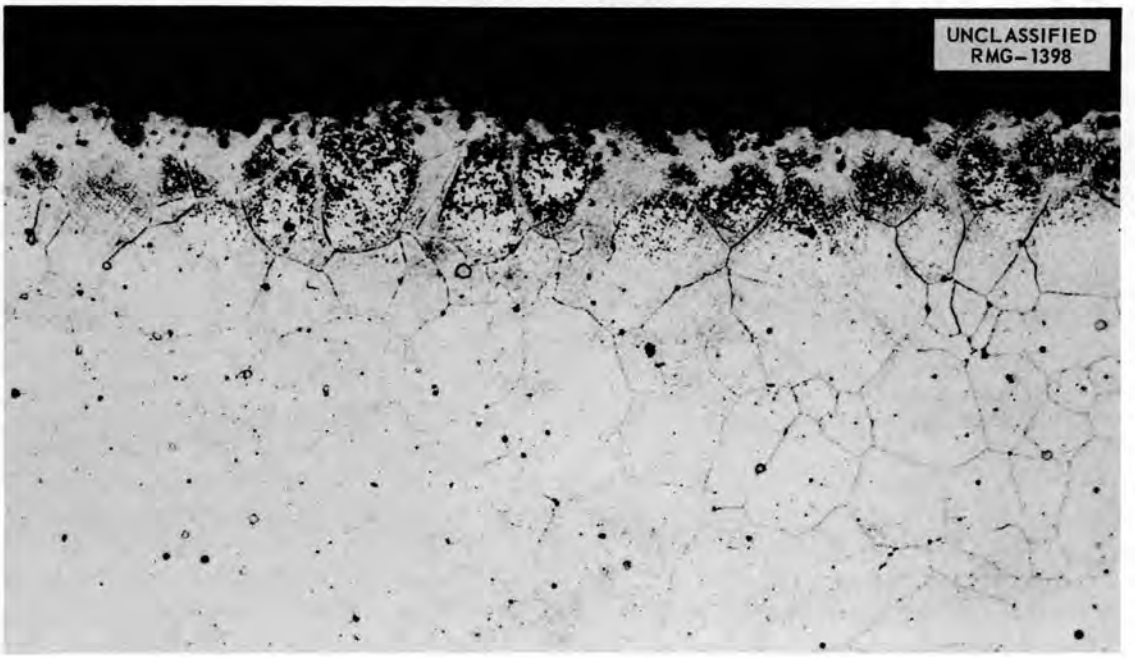

Fig. 8. Sample No. 304, Taken from Straight Section of Fuel Tubing Between Pump and Nose Coil Inlet at a Point 12 in. from the Pump of MTR In-Pile Loop 3. Intergranular corrosion to a depth of 0.5 mil can be seen. 250X. (Confidential with caption)

Fig. 9. Section Through Straight Sections of Fuel Tubing Between Nose Coil and Pump at a Point $22\frac{3}{4}$ in. from the Pump of MTR In-Pile Loop 5. The small-diameter tube that is full of fuel is the inlet line, and the small-diameter tube that has a shallow layer of fuel is the outlet line.

Examination of the fill tank, fill line, and vent line showed that the fuel in the fill line had frozen solid for the first $4\frac{1}{2}$ in. from the fill tank and that, from that point on, cavities had begun to appear in the fuel. The vent line appeared to be clear except for a few particles and a deposit close to the pump. The condition of the fuel in the fill line at the point of maximum fuel porosity, 1.6 in. from the pump, is shown in Fig. 10. The plug probably occurred in the fill line at this point, since the fuel found here was different in appearance from that found closer to the fuel tank where no porosity was observed. The condition of the fuel in the fill tank is shown in Fig. 11; the pump sump, which was void of fuel, is shown in Fig. 12. Thirteen fuel samples were obtained for chemical analysis at various locations around the loop. A radiograph of the fill tank, fill line, and vent line is shown in Fig. 13.

The fill-line Calrod heater failure was located and is shown in Fig. 14. The pump chattering was probably caused by rubbing of a wiper ring behind the flingers on the flinger shaft, Fig. 15. All the thermocouples in the nose-coil region appeared to be in operating condition. Thermocouple No. 28, which was at the rear of the fill line, could not be found. The cause of the leakage through the pump bulkhead could not be determined, since the glass seals may have been damaged during disassembly.[1]

[1] C. Ellis *et al.*, *Examination of ANP In-Pile Loop 5*, ORNL CF-56-7-48 (July 16, 1956).

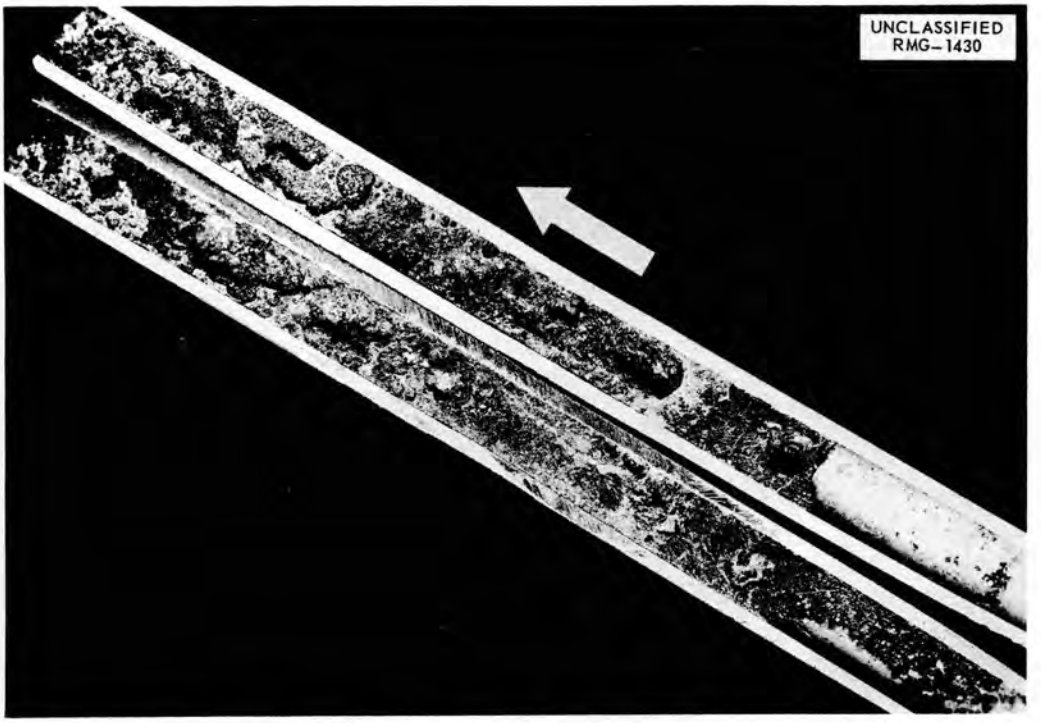

Fig. 10. Sectioned Fill Line, 3 in. Long, from Point at Which Maximum Fuel Porosity Is Shown in Fig. 13, 1.6 in. from Pump. 2.4X. Reduced 10%. ([redacted] with caption)

Fig. 11. Cap from Fill Tank of MTR In-Pile Loop 5 with Fuel in It. The hole in the cap is the vent line entrance. ([redacted] with caption)

Fig. 12. Pump Sump Shown Void of Fuel.

INVESTIGATION OF MATERIALS REMOVED FROM MTR IN-PILE LOOPS 3 AND 5

R. P. Shields

Chemical analyses of fuel and other materials from loop 3 have been made. A partially completed study of the results has been made, and the following conclusions can be drawn.

1. On the basis of analysis for iron, chromium, and nickel very slight, if any, corrosion occurred.
2. The amber-colored material found in the pump region is probably an oil decomposition product. This conclusion is based on the fact that the material is soluble in acetone, is waxlike in consistency, and has a fairly broad melting point of 225 ± 10°C.
3. Considerable amounts of Cs^{137} and Sr^{89} were deposited inside the copper lines leading to the fission-gas-adsorber trap.
4. There was evidence of oil deposits and the radioactivity was low in samples of carbon taken from the trap after they had been flushed with helium. The fission products Cs^{137} and Sr^{89} were present in the carbon in small amounts.

A more complete analysis of these results is being made.

Samples of fuel from loop 5 were extracted for analysis to determine the reason why it was not possible to fill this loop successfully.

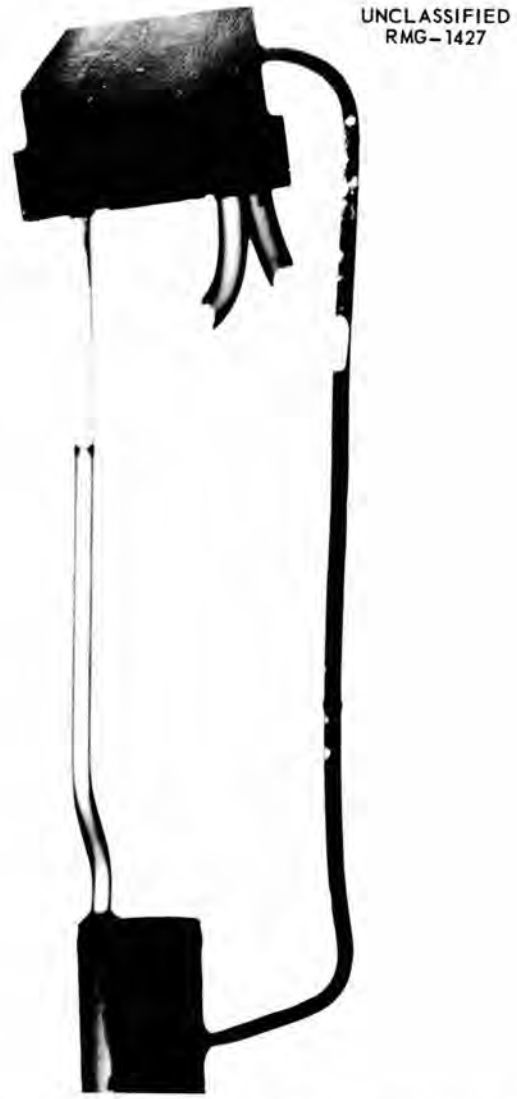

Fig. 13. Radiograph of Fill Tank, Fill Line, and Vent Line of MTR In-Pile Loop 5. ([redacted] with caption)

Fig. 14. Fuel Fill-Line Calrod Heater That Failed During Attempt to Fill MTR In-Pile Loop 5. ([redacted]ith caption)

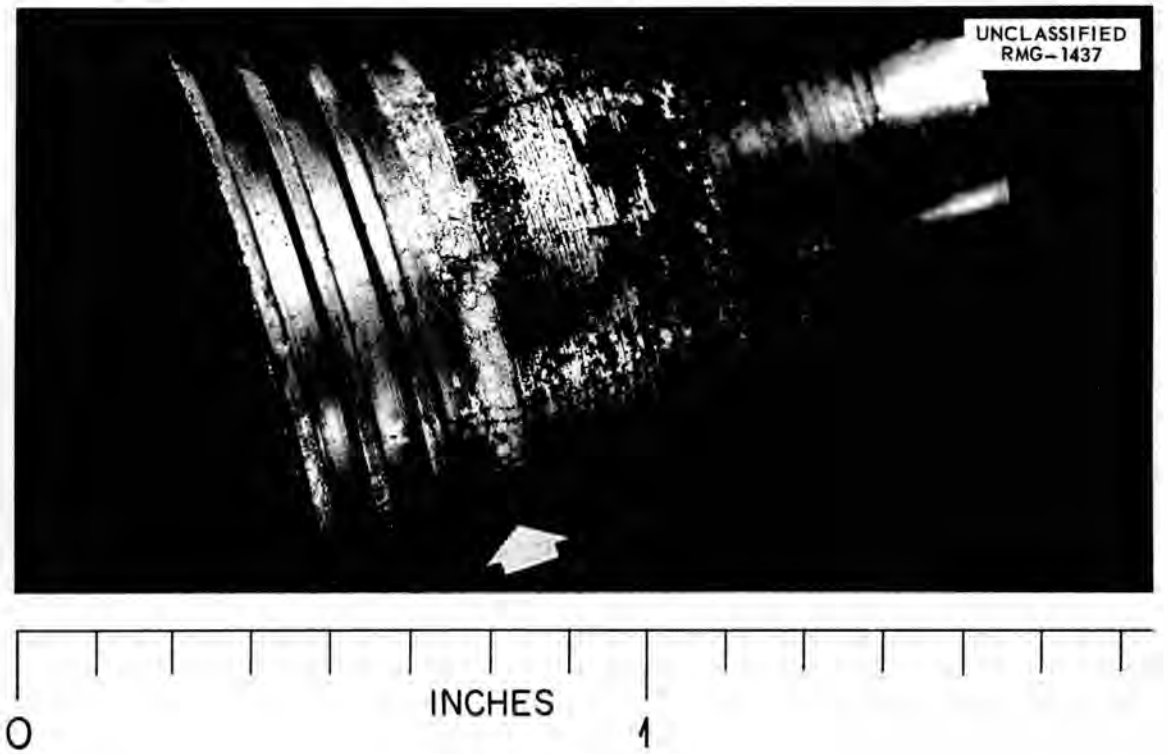

Fig. 15. Abraded Region on Pump Slinger Shaft That Was Caused by Rubbing of a Wiper Ring Behind the Slingers During Attempt to Fill MTR In-Pile Loop 5. (Confidential with caption)

EFFECT OF RADIATION ON STATIC CORROSION OF STRUCTURAL MATERIALS BY FUSED SALT FUELS

W. E. Browning H. L. Hemphill

The study of the effect of radiation on the corrosion of structural materials by fused salt fuels has continued. Two static Inconel capsules containing the fuel mixture $NaF-ZrF_4-UF_4$ (53.5-40-6.5 [redacted]) were irradiated in the MTR for over nine weeks at approximately 6 kw/cm^3. The capsules were at a temperature of 1570°F during the irradiation. Near the end of the test period a thermocouple failure led to a temperature excursion, as yet unevaluated, and one capsule released fission-product activity into the cooling-air off-gas line. By increasing the flow of coolant air enough to freeze the fuel, the radiation level at the top of the reactor resulting from the off-gas-line activity was reduced from 200 r/hr to 100 mr/hr without interruption of reactor operation. The radioactivity was confined to the off-gas system and there was no contamination of the air of the building. The irradiation of the other capsule was completed without incident. A second pair of capsules containing the same fuel mixture is being irradiated at 1500°F, for a planned exposure period of nine weeks.

Five Inconel capsules containing NaF, ZrF_4, and UF_4 or UF_3 that were previously irradiated have been opened, and samples have been submitted for chemical analysis and metallographic examination.

Hastelloy B capsules have been filled with an $NaF-KF-LiF-UF_4$ fuel mixture containing 5.8 mole % UF_4 and are being prepared for bench tests and MTR irradiation. The capsules are nickel-chromium plated on the outside surface to protect them from atmospheric oxidation.

Some improvements in design of the MTR-ORNL-2B irradiation facility have been accomplished. The capsule, shown in Fig. 16, is prepared in the same way as before; the test capsule is the part in the center of the photograph with the thermocouples attached. The separate part to the left is the sleeve which slips over the capsule and defines the cooling-air annulus. The three small flattened tubes carry the thermocouple wires into

the tube at the right. The complete length of the tube at the right can be seen in Fig. 17 with a compression spring on the other end. The thrust of the spring keeps the air annulus sleeve in place in a tapered seat in the outer tube shown at the top of Fig. 17. The outer tube has two parts, a $\frac{5}{8}$-in.-OD tube for the capsule and a $\frac{3}{8}$-in.-OD air-return tube. Both parts are welded to $\frac{3}{8}$-in.-OD air tubes which extend to the top of the reactor tank; the air-in tube carries the thermocouple leads. Each capsule is jacketed individually in this way. This assembly can be irradiated either in the B-4 facility or in one of the standard A positions in the MTR.

LITR VERTICAL IN-PILE LOOP

W. E. Browning

M. F. Osborne R. P. Shields
H. E. Robertson D. E. Guss[2]

The cause of the in-pile pump failure previously described[3] has been determined. A screw had come loose and lodged in the impeller, thus throwing it out of balance enough to bend the shaft. The bent shaft had rubbed against the impeller housing and stalled the motor. The screw served as a shear pin to prevent the impeller from unscrewing from the shaft. The shaft was peened around the screw to hold it in place. It is not known why the peening failed to hold the screw. This method of fastening various internal parts will be replaced by welding in future loop fabrication.

Tests have been continued on a modified pump for use in future loops. The modified motor and pump assemblies are shown in Fig. 18. The modifications include precision bearings, a shorter and stiffer shaft, a greater clearance around the impeller, and an enlarged pump exhaust port. An

[2]On assignment from the United States Air Force.

[3]W. E. Browning *et al.*, *ANP Quar. Prog. Rep. June 10, 1956*, ORNL-2106, p 238.

UNCLASSIFIED
PHOTO 17339

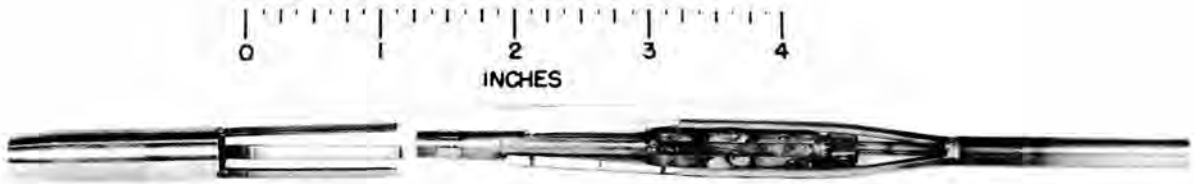

Fig. 16. Inconel Capsule and Associated Equipment for MTR Irradiation.

UNCLASSIFIED
PHOTO 17340

Fig. 17. Equipment, Including Outer Jacket, for Irradiation of Inconel Capsules in the MTR.

Fig. 18. Modified Motor and Pump for Use in LITR Vertical In-Pile Loop. (*a*) Impeller and shaft components. (*b*) Pump assemblies. (*c*) Motor parts.

improved radiation-resistant grease recently developed by California Research Corporation has become available for use in future operation.

High-temperature tests of the new shaft have led to a design in which the highest bearing-part temperature is 105°C, even when the temperature of the shaft where it enters the fuel is as high as 950°C. These temperatures are for a stationary shaft; the bearing temperature for a rotating shaft will be lower because of heat transfer by the rolling balls. The over-all shaft overhang is only 4 in., of which $1\frac{3}{4}$ in. is in the fuel. The new shaft with the impeller is shown in Fig. 18*a*. Longitudinal conductive heat transfer is suppressed by use of a hollow shaft and the four rows of radial holes visible in Fig. 18*a*. Radial heat transfer from the shaft to the lower bearing is decreased by a set of longitudinal grooves, which reduce the area of contact between the shaft and the lower bearing. This distributes the heat flux more equally between the two bearings and thus reduces the temperature of the inner race of the lower bearing.

Bearing tests have been run in helium under simulated conditions of temperature and heat flux with both the new and old radiation-resistant lubricants. The satisfactory performance obtained under these conditions indicates that the bearing clearance is sufficient for the design thermal gradient through the bearing and that the bearing temperatures are not so high that the grease will be damaged in the absence of radiation.

In the design of the pump a compromise had to be made on impeller clearance. It was desired that the clearance be large enough to ease the shaft alignment but not large enough for leakage to occur and reduce pump efficiency. Hydraulic pump performance tests have been run to optimize this design choice. Impeller clearances have been increased from a range of 0.010 to 0.020 in. at various positions to 0.050 to 0.070 in. This increase caused a measurable but unimportant decrease in pump efficiency. The pump performance tests were run with water in a plastic model of the pump. The test apparatus is shown in Fig. 19. The flow-throttling valve is used for adjusting the load on the pump. The fluid level in the pump is adjusted by means of the cylindrical reservoir. The pump speed is regulated by the motor control panel and is measured by the electronic tachometer. Test results are given in Fig. 20, which shows the pump pressure as a function of flow for

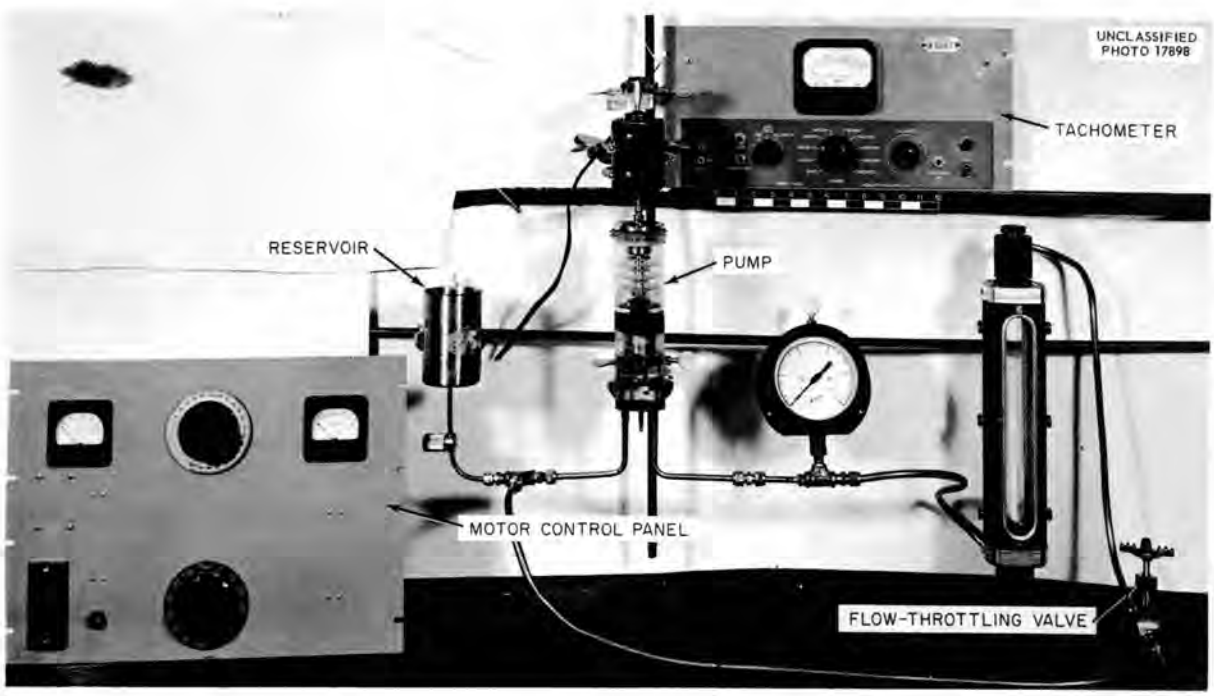

Fig. 19. Apparatus for Testing Pump Performance.

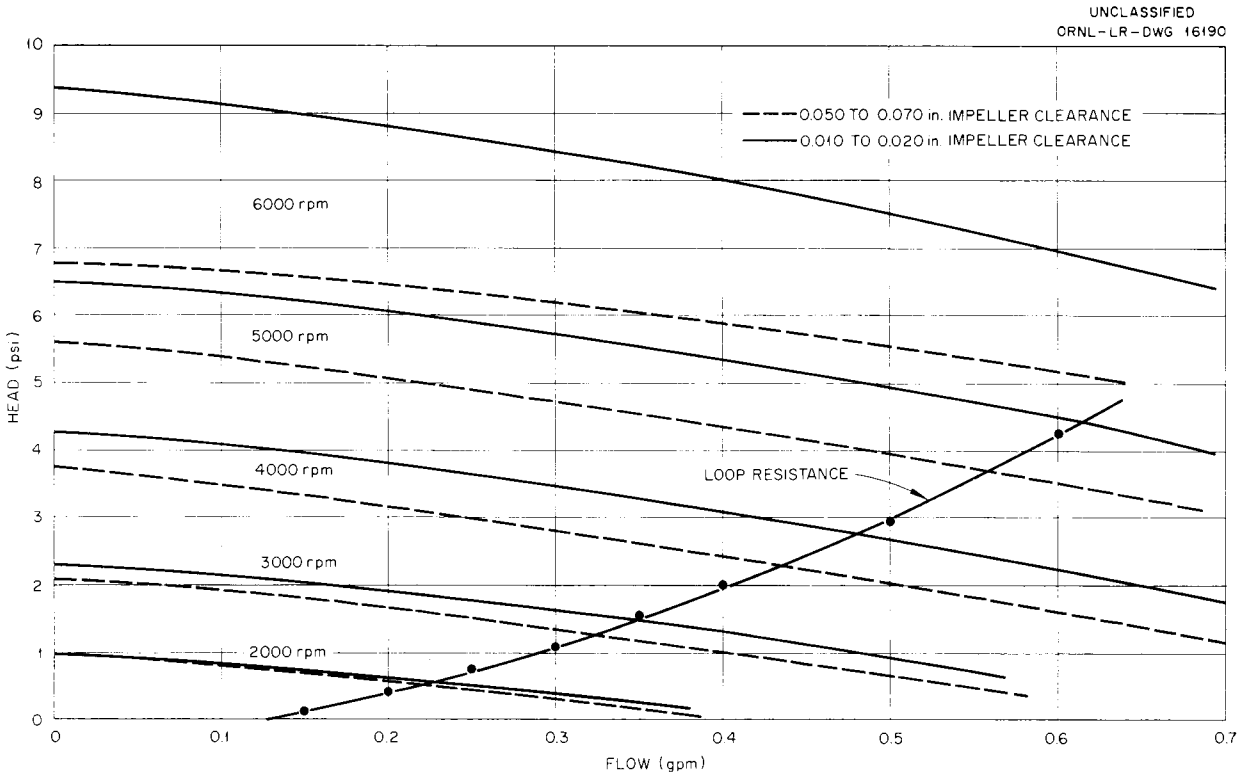

Fig. 20. Performance Curves with Water for Modified Pump for LITR Vertical In-Pile Loop Before and After Impeller Clearances Were Increased.

water before and after the increase in clearance for various pump speeds. Figure 20 also shows the resistance curve representing the loop for water. Both sets of curves are for pumps having a larger exit port than was formerly used. The results of the two changes are approximately equal and opposite at the design point; so the pump is still operated at about the same speed.

The pressure vs flow data obtained with water were converted to fuel conditions by the method described by Willis *et al.*[4] Recent values for the viscosity of the fuel were used to obtain the data in Fig. 21, which gives the Reynolds number for the fuel in the LITR vertical in-pile loop as a function of the pump speed.

A full-scale Inconel pump has been assembled that is identical to pumps to be used in the Inconel in-pile loops. It will be filled with depleted fuel and run in the laboratory under conditions as

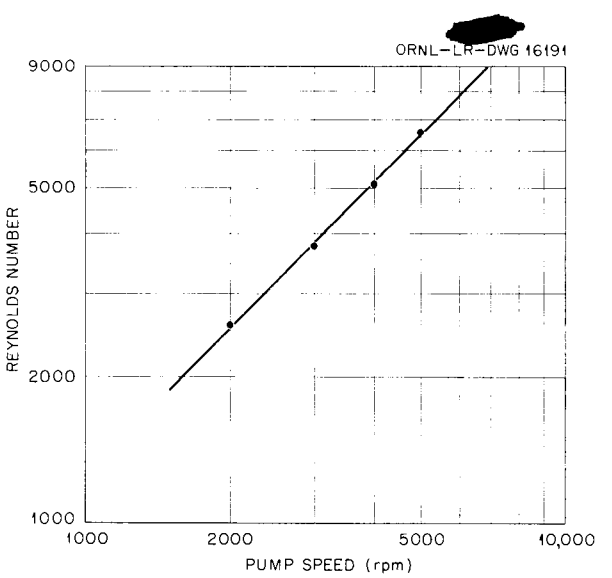

Fig. 21. Estimated Reynolds Number of the Fuel Mixture in LITR Vertical In-Pile Loop as a Function of Pump Speed.

[4]W. R. Willis *et al.*, *Solid State Semiann. Prog. Rep. Aug. 31, 1955*, ORNL-1944, p 16.

nearly like those in the reactor as possible. Existing parts for in-pile loops are being modified to incorporate these recent changes.

ART OFF-GAS SYSTEM INSTRUMENTATION ANALYSIS

W. E. Browning R. P. Shields

Preparations are being made for investigating the resolution, sensitivity, and general performance of scintillation gamma-ray spectrometers of the type to be used on the ART off-gas system. The purpose of the tests will be to determine the limitations that might result from the rather drastic departure which must be made from conventional spectrometer geometry because of the high intensity of the source.

DESIGN CALCULATIONS FOR THE VERTICAL MINIATURE IN-PILE LOOP

M. T. Robinson J. F. Krause[5]

An extensive series of design calculations for the LITR vertical miniature in-pile fuel loop was previously reported.[6] In an appendix to that report,[7] a method was presented for making such calculations by electronic analog simulation. The method was based on partial analytical solution of the differential equations describing the heat balance in the loop, followed by analog computation, supported by some desk machine computation. The correct solutions were then found by interpolation among a family of analog computer results. A much-improved method of analog computation is presented here which eliminates the interpolation procedure and the desk machine work, as well as substantially shortening the amount of analog computation required to obtain correct solutions.

The differential equations employed are

$$\frac{dT_f}{ds} = \frac{\beta_1'\phi - \alpha_2' y}{(Ref)}, \tag{1}$$

$$\frac{dT_a}{ds} = \frac{\alpha_3' y}{(Rea)}, \quad \text{for } 0 \le s \le \frac{S}{2}, \tag{2a}$$

$$\frac{dT_a}{ds} = \frac{-\alpha_3' y}{(Rea)}, \quad \text{for } \frac{S}{2} \le s \le S, \tag{2b}$$

$$T_f - T_1 = \gamma_1 y, \tag{3}$$

$$T_1 - T_2 = \gamma_2 y, \tag{4}$$

$$T_2 - T_a = \gamma_3 y, \tag{5}$$

where all symbols have been previously defined,[6] except that the factor $(Ref)^{-1}$ has been removed from β_1 and α_2 and the factor $(Rea)^{-1}$ from α_3 to form the primed quantities. The initial and boundary conditions may be expressed as

$$T_f(s = 0) = T_f(s = S) = T_f^0 \quad \text{(a constant)}, \tag{6}$$

$$T_a(s = 0) = T_f(s = S) = T_a^0 \quad \text{(a constant)}, \tag{7}$$

$$\lim_{\epsilon \to 0} T_f\left(s = \frac{S}{2} - \epsilon\right) = \lim_{\epsilon \to 0} T_f\left(s = \frac{S}{2} + \epsilon\right). \tag{8}$$

Since the flux function $\phi(s)$ is symmetrical about $S/2$, the discontinuities in the functions T_1, T_2, T_a, and y at the point $S/2$ may be calculated when the values of all quantities on one side of the discontinuity are known. This calculation was done on a desk machine in the previous work. However, the work may be simplified by reversing the direction of integration in the region $S/2 \le s \le S$, making use of boundary condition (Eq. 8) to establish the correctness of a result, rather than using Eqs. 6 and 7 as was done before. Elimination of the extrapolation procedure results from using Eqs. 1 through 5 directly, rather than solving them to find a differential equation in y and establishing the analog in terms of the new equation.

The analog is established by replacing the space coordinate, s, in Eqs. 1 through 5 by time coordinates, t_1 and t_2, such that for $0 \le s \le S/2$, $0 \le t_1 \le \tau$; and for $S/2 \le s \le S$, $\tau \ge t_2 \ge 0$.

[5] On loan from Pratt & Whitney.

[6] M. T. Robinson and D. F. Weekes, *Design Calculations for a Miniature High-Temperature In-Pile Circulating Fuel Loop*, ORNL-1808 (Sept. 19, 1955).

[7] E. R. Mann, F. P. Green, and R. S. Stone, *An Appendix on Analog Simulation*, Appendix B, ORNL-1808.

The equations then become:

Region $0 \leq s \leq \frac{S}{2}$

$$\frac{dT_f}{dt_1} = \frac{\beta_1'\phi - \alpha_2'y}{(Ref)}$$

$$\frac{dT_a}{dt_1} = \frac{\alpha_3'y}{(Rea)}$$

$$T_f - T_1 = \gamma_1 y$$

$$T_1 - T_2 = \gamma_2 y$$

$$T_2 - T_a = \gamma_3 y$$

Region $\frac{S}{2} \leq s \leq S$

$$\frac{dT_f}{dt_2} = -\frac{\beta_1'\phi - \alpha_2'y}{(Ref)}$$

$$\frac{dT_a}{dt_2} = \frac{\alpha_3'y}{(Rea)}$$

$$T_f - T_1 = \gamma_1 y$$

$$T_1 - T_2 = \gamma_2 y$$

$$T_2 - T_a = \gamma_3 y$$

The initial conditions are

$$T_f(t_1 = 0) = T_f(t_2 = 0) = T_f^0$$

$$T_a(t_1 = 0) = T_a(t_2 = 0) = T_a^0$$

For a given value of (Ref), the fuel Reynolds number, computations are repeated, with successive values of (Rea), the air Reynolds number, being used, until

$$T_f(t_1 = \tau) = T_f(t = \tau) \ .$$

The block diagram of the electronic analog simulator is shown in Fig. 22. Scale factors are chosen such that the voltages are related to the physical variables by the relations:

$$V(T_{f,1,2, \text{ or } a}) = 10^{-1}T_{f,1,2, \text{ or } a} \ ,$$

$$V(\phi) = \phi \ ,$$

$$V(y) = \frac{y}{k} \ .$$

The last choice is required in order that the calculation will be sufficiently flexible for all combinations of (Ref) and (Rea) to be made accessible.

A voltage proportional to the neutron flux is available from the output of the potentiometer labeled "n". Variation in this voltage allows simulation of variations in the flux depression caused by the loop. The circuit elements preceding potentiometer "n" determine the time scale and amplitude of the variation of the flux with time. The flux-voltage is fed through a potentiometer to one input of amplifier 1, producing there a voltage proportional to $\beta_1'\phi$. Signals proportional to $-y$ and $+y$ are available from the outputs of amplifiers 4 and 11, respectively. The former is fed through two potentiometers to the second input of amplifier 1, producing there a voltage proportional to $-\alpha_2'y$. The output of amplifier 1 may be taken directly, corresponding to the first half of the loop $(0 \leq s \leq S/2)$, or may be reversed by amplifier 13, corresponding to the other half $(S/2 \leq s \leq S)$. This choice is made by the function switch F_1, the appropriate signal being fed through a potentiometer to the input of amplifier 2, where it produces a voltage proportional to $-\dot{T}_f$. Since amplifier 2 is an integrator, a time-dependent device, its time constant must be chosen to correspond with the desired value of τ. In this case, two inputs are used in parallel as a convenient choice of this time constant. Thus τ is determined as $S/4$ sec, where S is the total length of the loop in centimeters. The output of amplifier 2 is proportional to T_f. Amplifiers 6 and 8 perform the operations

$$T_f - \gamma_1 y = T_1$$

and

$$T_1 - \gamma_2 y = T_2 \ ,$$

respectively. The output of amplifier 11 is fed through three potentiometers to the input of amplifier 5, producing there a signal proportional to T_a. This amplifier, with the same time constant as amplifier 2, produces a voltage proportional to $-T_a$. Amplifier 10 and the following potentiometer perform the operation

$$\frac{T_2 - T_a}{\gamma_3} = y \ .$$

Amplifier 11 is required to prevent variations in the behavior of the potentiometer labeled "$10/k\gamma_3$" by other parts of the circuit. Amplifiers 3, 7, 9, and 12 provide zero suppression for convenient recording of T_f, T_1, T_2, and y, respectively.

This new circuit has been used to make calculations of the behavior of the Mark VIII loop[6] when circulating fluoride fuel No. 41 in position C-46 of the LITR. The flux data are those previously

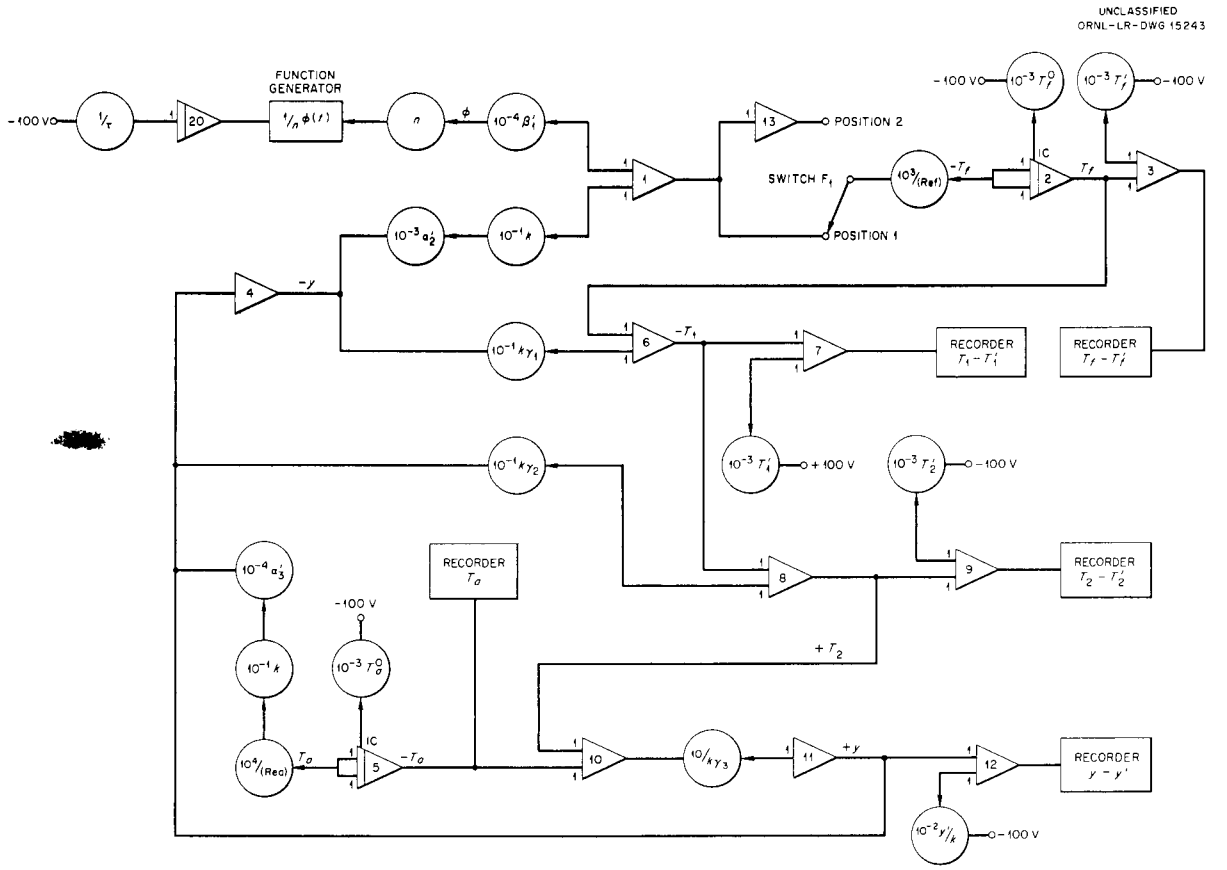

Fig. 22. Block Diagram of Electronic Analog for Heat Transfer Simulation of the Miniature Vertical In-Pile Loop.

reported[8] for that position. The physical property data for air are the same as before.[6] The physical property data for fuel 41 are given below:

Composition	$NaF\text{-}ZrF_4\text{-}UF_4$ (63-25-12 mole %)
Viscosity	4.3 centipoises
Specific heat	1.0 joule/g·°C
Thermal conductivity	0.014 watt/cm·°C
Density	3.38 g/cm^3

The loop was considered to be located with its tip at the mid-plane of the LITR. The flux was assumed to be depressed 50% by the presence of the loop. The initial air temperature, T_a^0, was always taken as 30°C.

[8] M. T. Robinson, *Solid State Semiann. Prog. Rep. Feb. 28, 1954*, ORNL-1677, p 27.

Some results of the calculations are summarized in Tables 1 and 2 and in Figs. 23 and 24. Figure 23 shows typical profiles of the temperatures T_f (mixed-mean fuel temperature), T_1 (fuel-metal interface temperature), and T_2 (metal-air interface temperature), and Fig. 24 shows profiles of T_a (air temperature) and of y (heat transfer function). The discontinuities occurring in the plots of T_1, T_2, T_a, and y result from the use of two separate cooling-air streams. Local heat flow would be expected to remove these discontinuities in the real loop. The very different shapes of T_f and of T_1 and T_2 are notable (Fig. 23). This feature is important in analyzing experimental data, since T_2 is the only quantity which can be directly measured. The effect of initial fuel temperature (T_f^0) on other quantities is shown in Table 1. As was realized before,[6] ΔT_f is very little affected by changes in T_f^0. It should be noted, however, that

TABLE 1. EFFECT OF INITIAL FUEL TEMPERATURE ON COOLING-AIR REQUIREMENTS FOR $(Re_f) = 4000$

Fuel composition 41 at 50% of flux, LITR position C-46

T_f^0 (°C)	(Re_a)	T_1^0	T_2^0	ΔT_f (°C)	ΔT_1 (°C)	ΔT_2 (°C)
750	34,500	659	641	87	81	83
800	31,500	708	690	88	83	85
850	29,750	756	738	89	85	86

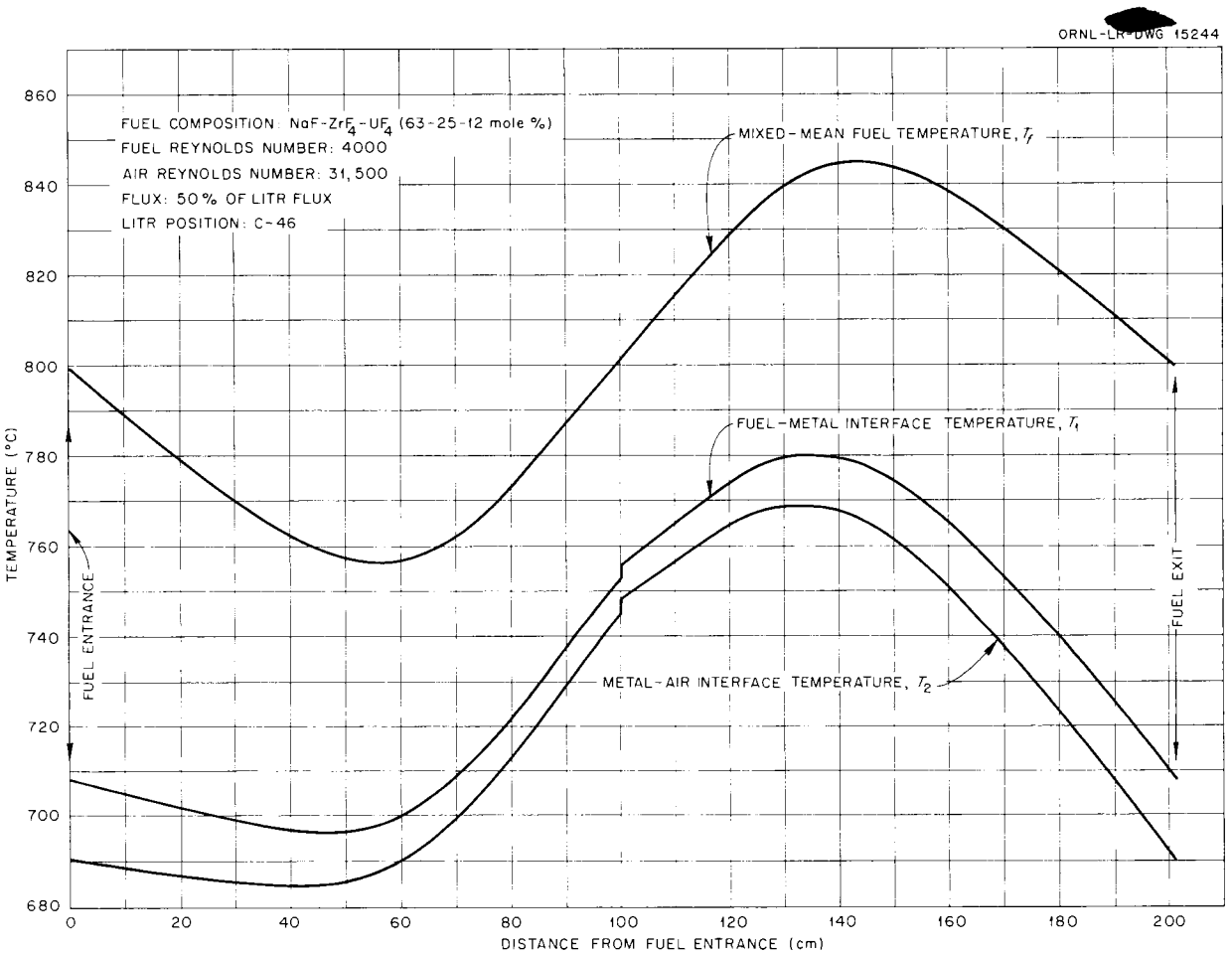

Fig. 23. Calculated Temperature Profiles for LITR Vertical In-Pile Loop (Mark VIII).

TABLE 2. EFFECTS OF FUEL FLOW RATE ON COOLING-AIR REQUIREMENTS FOR $T_f^0 = 800°C$

Fuel composition 41 at 50% of flux, LITR position C-46

(*Ref*)	(*Rea*)	T_1^0 (°C)	T_2^0 (°C)	ΔT_f (°C)	ΔT_1 (°C)	ΔT_2 (°C)
2,000	46,000	477	460	163	134	139
3,000	34,000	650	632	114	104	106
4,000	31,500	708	690	88	83	85
6,000	29,500	751	732	59	57	58
8,000	29,000	764	746	44	43	45
10,000	29,000	770	752	36	35	36

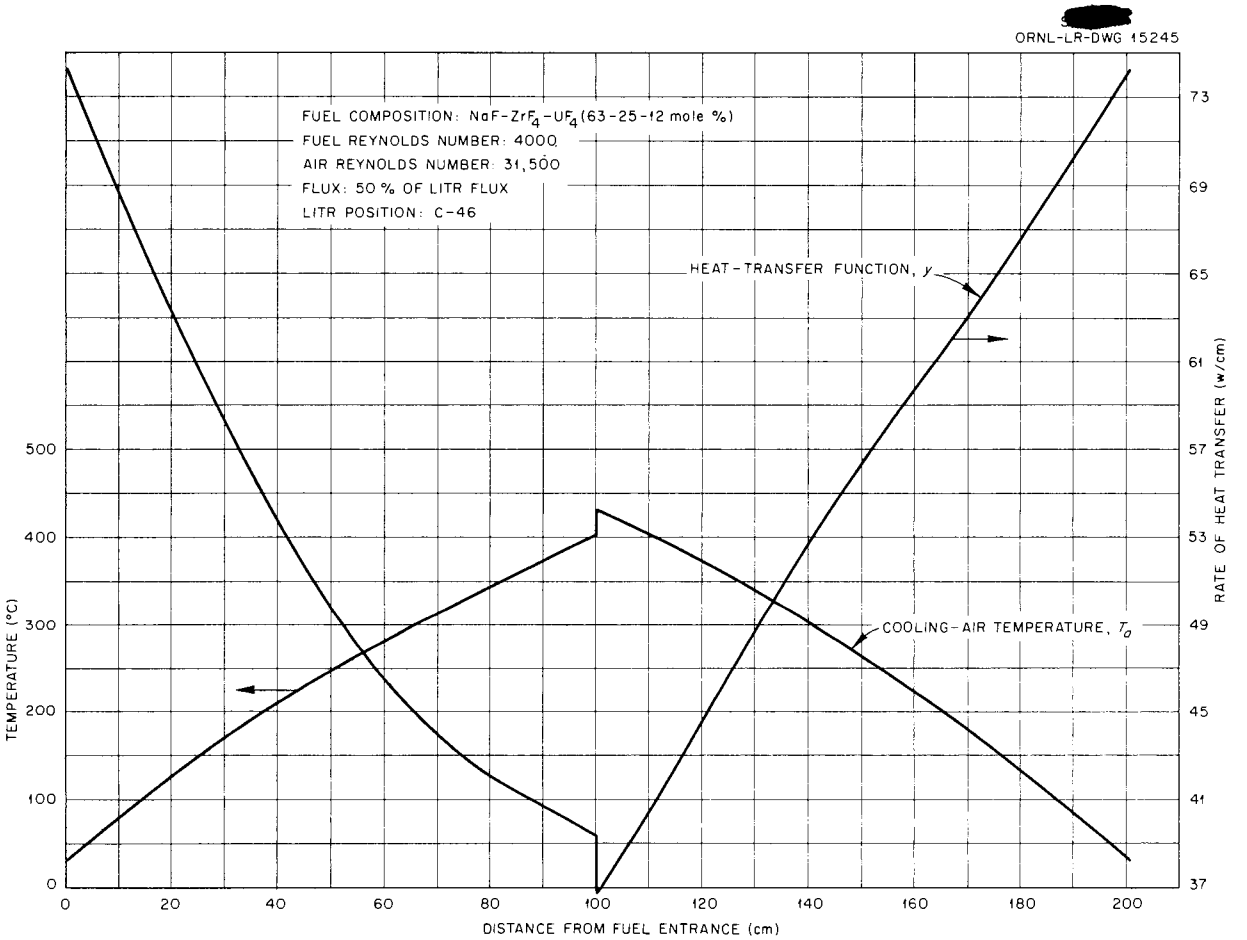

Fig. 24. Calculated Air-Temperature and Heat-Transfer-Function Profiles for LITR Vertical In-Pile Loop (Mark VIII).

appreciable changes in cooling-air requirements are associated with changes in T_f^0. Table 2 illustrates the effect of fuel flow rate on other quantities. The important points to notice are the close similarity of the values ΔT_2 and ΔT_f, except at the lowest fuel Reynolds numbers; the small difference between T_1^0 and T_2^0; and the large difference between T_f^0 and T_1, especially at lower flow rates. The first point suggests that experimental values of ΔT_2 may be used without correction to characterize fuel "ΔT". The second point results from the fairly small heat extraction rate, around 30 w/cm^2 or less. The third point is most important in assessing corrosion results.

ART REACTIVITY TRANSIENTS ASSOCIATED WITH FLUCTUATIONS IN XENON-REMOVAL [redacted] EFFICIENCY

M. T. Robinson J. F. Krause

The possibility has been investigated that fluctuations in efficiency of the ART xenon-removal equipment might lead to troublesome transients in reactivity. The calculations previously reported[9] have been extended for this purpose. Since only short times are of interest here, the equations may be simplified to

$$\dot{x} = \lambda_f(\alpha_2 y - x) , \tag{1}$$

$$\dot{y} = \beta\lambda_f(x - \alpha_2 y) - \lambda_g y = -\beta\dot{x} - \lambda_g y , \tag{2}$$

where

x = Xe^{135} poisoning in the fuel,
y = "equivalent poisoning" in the gas phase,
α_2 = RTS, the product of the universal gas constant, R, times the absolute temperature, T, times the solubility coefficient of xenon in fuel, S,
β = ratio of volume of fuel to volume of gas phase,
λ_f = rate constant for transfer of xenon from fuel to gas,
λ_g = rate constant for removal of xenon from system by off-gas flow.

Equations 1 and 2 were solved with an electronic analog computer by using the block diagram shown in Fig. 25. The output of amplifier 1 is a voltage proportional to $\dot{x}$. This voltage is integrated in amplifier 2, the initial condition on the integration being set by the potentiometer "$0.2x_0$." A voltage proportional to x is fed to the recorder and to one input of the summing amplifier 4. The output of amplifier 1 is also fed through the potentiometer labeled "$\alpha_2\beta$" to one input of the summer-integrator, amplifier 3. The output of amplifier 3 is fed back through the potentiometer labeled "λ_g" to a second input of amplifier 3. This amplifier thus performs the operation

$$\alpha_2\beta\dot{x} + \alpha_2\lambda_g y = -\alpha_2\dot{y}$$

and then integrates y, subject to the initial condition set by the potentiometer "$0.2\alpha_2 y_0$." A voltage proportional to $\alpha_2 y$ is fed from amplifier 3 to the second input of amplifier 4. The output of amplifier 4, proportional to $(\alpha_2 y - x)$, is fed through potentiometer "λ_f" to the input of amplifier 1. In analyzing Fig. 25, it should be noted that, in addition to performing the appropriate mathematical operation, each amplifier inverts the phase of the input voltage.

Scale factors for the computation were selected such that all constants had their true values. The scale chosen for x and y was such that 1% poisoning was represented by 20 v. The recorder could be used with either 20 v (1%) or 100 v (5%) full-scale settings. Real time was used throughout the computation. The data employed were taken from the previous report,[9] subsequent modifications in ART design being considered more or less irrelevant. It was assumed that the reactor had reached xenon equilibrium under conditions specified by selected values of λ_f and λ_g, which allowed calculation of x_0 and y_0 from the steady-state relations given before.[9] At the start of a calculation, either λ_f or λ_g was assumed to change very rapidly to a new value, and the change in x was plotted during an interval of time up to 2 min. The results obtained are given in Table 3. For each case the initial slope, $-(dx/dt)_0$, and the initial period, $x_0/(dx/dt)_0$, are given. Some typical results are plotted in Fig. 26.

Examination of Table 3 shows that the initial period is essentially independent of λ_g and of changes in λ_g, however large. The period decreases with increasing λ_f, whether the disturbance is a change in λ_f or in λ_g. In no case is the period sufficiently short to cause concern for the controllability of the ART. The compensating effects

[9] M. T. Robinson, *A Theoretical Study of Xe^{135} Poisoning Kinetics in Fluid-fueled, Gas-sparged Nuclear Reactors*, ORNL-1924 (Feb. 6, 1956).

UNCLASSIFIED
ORNL-LR-DWG 15241

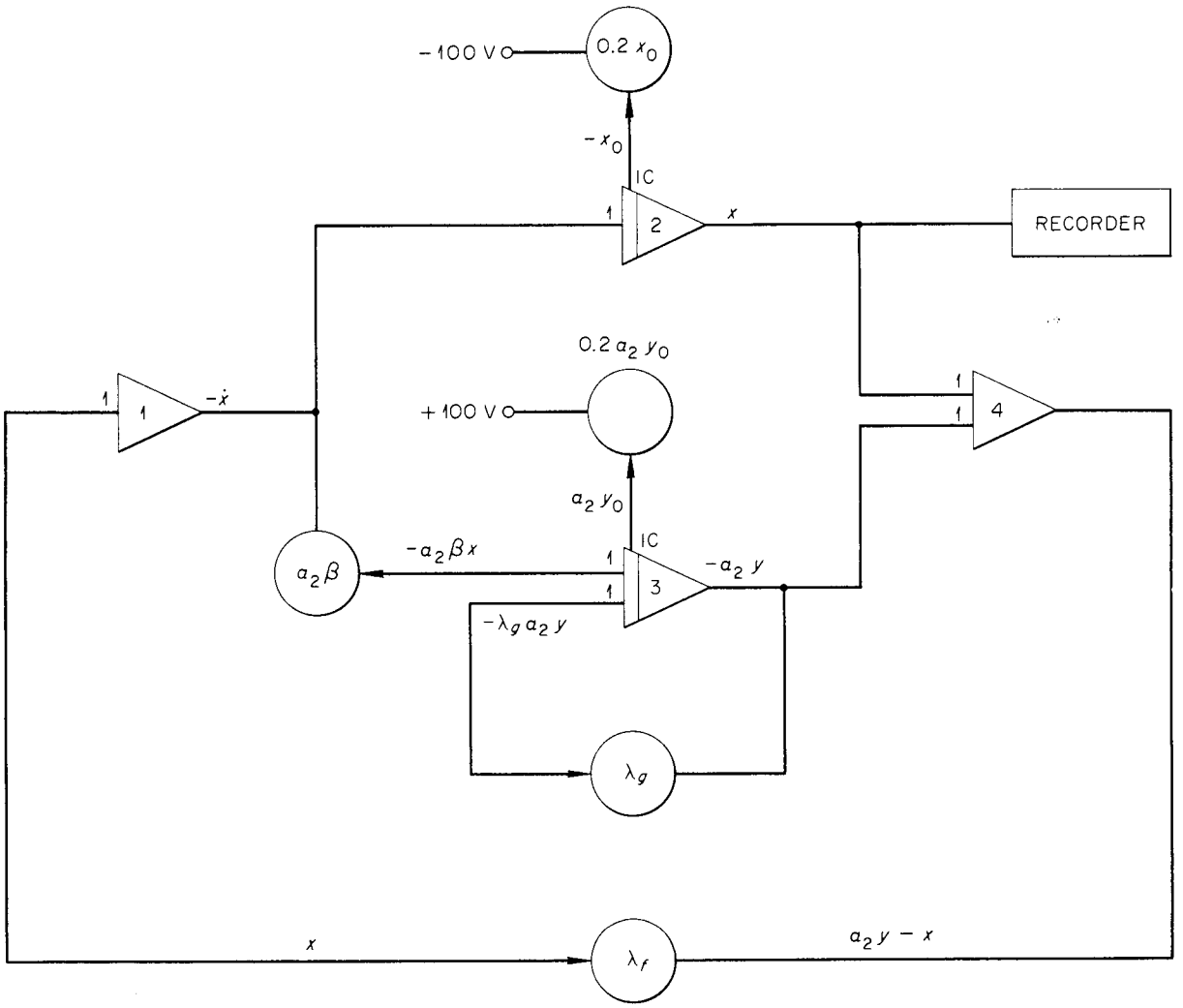

Fig. 25. Block Diagram of an Electronic Analog Simulator for the Equations $\dot{x} = \lambda_f(a_2 y - x)$ and $\dot{y} = \beta\lambda_f(x - a_2 y) - \lambda_g y$.

TABLE 3. INITIAL INCREASES IN ART REACTIVITY FOLLOWING FLUCTUATIONS IN XENON-REMOVAL EFFICIENCY

x_0 (%)	λ_f (sec^{-1})		λ_g (sec^{-1})*		Initial Slope (%/sec)	Initial Period (sec)
	$t < 0$	$t > 0$	$t < 0$	$t > 0$		
3.98	1	1	0	0.025	1.44	3
3.98	0.5	0.5	0	0.025	1.54	3
3.98	0.1	0.1	0	0.025	0.35	11
3.98	0.05	0.05	0	0.025	0.19	21
3.98	0.01	0.01	0	0.025	0.037	106
3.98	0.005	0.005	0	0.025	0.019	206
0.74	0.001	0.01	0.025	0.025	0.0069	106
0.74	0.001	0.1	0.025	0.025	0.063	12
0.74	0.001	1	0.025	0.025	0.27	3
0.75	0.001	0.01	0.015	0.015	0.0072	105
0.75	0.001	0.1	0.015	0.015	0.067	11
0.75	0.001	1	0.015	0.015	0.27	3
0.82	0.001	0.01	0.005	0.005	0.0075	109
0.82	0.001	0.1	0.005	0.005	0.071	12
0.82	0.001	1	0.005	0.005	0.27	3
0.97	0.001	0.01	0.002	0.002	0.0095	102
0.97	0.001	0.1	0.002	0.002	0.080	12
0.97	0.001	1	0.002	0.002	0.26	4
3.98	0.001	0.01	0	0	0.038	104
3.98	0.001	0.1	0	0	0.35	11
3.98	0.001	1	0	0	1.44	3

*The sparging gas flow rate is v_g (STP liters/day) $= 2.27 \times 10^5 \lambda_g$ (sec^{-1}).

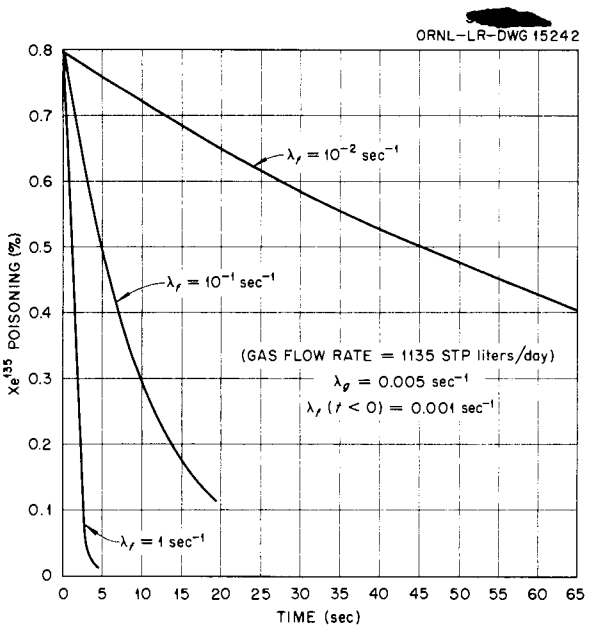

Fig. 26. Change in Xe^{135} Poisoning in ART Following a Change in Phase-Transfer Rate Constant.

of the delayed neutrons and of the negative temperature coefficient of the reactor are sufficient to overcome fluctuating behavior of xenon-removal equipment.

USE OF Zr^{95} AS A FISSION MONITOR

W. A. Brooksbank, Jr.[10]

It has been found that the use of Cs^{137} as a monitor for U^{235} fission in ANP fluoride fuels is not entirely satisfactory because of possible loss of its parent, 3.9-min Xe^{137}. As a substitute, 65-day Zr^{95} has been suggested. In order to calibrate the use of this isotope, two samples of enriched uranium were irradiated as solutions for 2.375 days in hole 10 of the ORNL Graphite Reactor. One solution was prepared from U_3O_8, the other from fluoride fuel composition. After the samples were allowed to decay for ten days, radiochemical determinations were made of Cs^{137} and of Zr^{95}. From these results the fission yield of Zr^{95} was calculated to be 0.0664 ± 0.0013 atom/fission. If the fission yield is calculated from the radiochemical Zr^{95} analyses and from the cobalt activation neutron flux observed from a monitor irradiated with the samples, the result obtained is 0.0632 ± 0.0021 atom/fission. The discrepancy between the two results is removed when the cobalt activation flux is corrected for the cadmium ratio prevailing in hole 10 (about 30). The fission yield recommended for use in fission monitoring with Zr^{95} is 0.0664 ± 0.0013 atom/fission.

[10] Analytical Chemistry Division.

HOT METALLOGRAPHY

A. E. Richt
E. J. Manthos W. B. Parsley
J. O. Stiegler E. D. Sims
R. M. Wallace R. N. Ramsey
C. Ellis

Metallographic examination of specimens submitted by the Radiation Corrosion Group of the Homogeneous Reactor Project has continued. Examination of the Zircaloy-2 corrosion coupons from in-pile loop FF has been completed, and the results have been reported.[1] Examination of components, coupons, and stress-corrosion specimens from HRP in-pile loop EE has been completed, and the results have been reported.[2] Examination of components from the North Carolina State College Reactor has been completed and reported.[3,4] Additional specimens consisting of in-pile loop control valves and corrosion pins from in-pile static bomb tests have also been examined and the results reported.[5] Metallographic examination of in-pile loops L-4-8 and L-4-11 is now in progress. Two additional loops (GG and L-4-12) have been disassembled and are being held for future metallographic examination.

Postirradiation examination of a series of small fuel plates for the APPR Project has begun.[6] At the present time, examination of 14 of the total of 26 plates in this phase of the experiment has been completed. Examination of the remaining plates is contemplated in the near future. Examination of sections of fuel plates from a full-size APPR-type fuel element which was irradiated in the MTR has also been initiated, and completion is contemplated shortly.

Examination of ANP in-pile loop 3 has been completed, and preliminary results have been reported.[7,8] A final report is now being compiled and will be issued in the near future. Failure of in-pile loop 5 resulted in the request for disassembly in order to determine why the loop could not be filled successfully after it was inserted in the MTR. No evidence of a mechanical or metallic plug was noted in disassembly. However, the fill line contained a substance entirely different in physical appearance from that of the normal fuel mixture.[9] Chemical analysis of samples of this material indicated that the fuel contained a high percentage of zirconium oxide. No metallographic examination was attempted on this loop, since it had not been operated. Disassembly and metallographic examination of specimens from ANP in-pile loop 4 are now in process.

A recent breakdown of the remotely controlled metallographic cutoff machine drastically demonstrated the need for more reliable and more easily decontaminated hot-cell equipment. Failure of this machine resulted, essentially, in the remote preparation of metallographic specimens being halted for six weeks while attempts were being made to decontaminate this instrument to a level that mechanical repairs could be made.

---

[1] A. E. Richt and J. O. Stiegler, *Metallographic Examination of Zircaloy II Coupons from H.R.P. In-Pile Loop (FF)*, ORNL CF-56-8-48 (Aug. 8, 1956).

[2] A. E. Richt, *Metallographic Examination of H.R.P. In-Pile Loop (EE) Components and Coupons*, ORNL CF-56-7-17 (July 6, 1956).

[3] A. E. Richt, *Metallographic Examination of Components from the North Carolina State College Reactor*, ORNL CF-56-3-158 (March 30, 1956).

[4] A. R. Olsen and A. E. Richt, *Examination of the North Carolina State College Reactor Core*, ORNL CF-56-6-115 (July 20, 1956).

[5] W. B. Parsley, A. E. Richt, and E. D. Sims, *Metallographic Examination of H.R.P. In-Pile Loop Valves V-2, V-15, and Zircaloy II Pin from Bomb Z-14*, ORNL CF-56-7-2 (July 3, 1956).

[6] F. H. Neill, *Irradiation of Stainless Steel Fuel Element Samples in MTR-Irradiation Request ORNL-21*, ORNL CF-55-4-153 (April 26, 1955).

[7] M. J. Feldman *et al.*, *ANP Quar. Prog. Rep. March 10, 1956*, ORNL-2061, p 183–187.

[8] E. J. Manthos *et al.*, *ANP Quar. Prog. Rep. June 10, 1956*, ORNL-2106, p 234.

[9] C. Ellis *et al.*, *Examination of ANP In-Pile Loop 5*, ORNL CF-56-7-48 (July 16, 1956).

HOT-CELL OPERATION

S. E. Dismuke E. S. Schwartz

Postirradiation testing and metallographic analysis were continued on APPR-type fuel element samples. The details of this analysis will be published at a later date.

The LITR vertical in-pile loop reported previously[1] was not operated at full power in the LITR because of mechanical failure of the pump. The loop was sectioned and examined, and the fuel salt was melted out in the Solid State Division hot cells. The results of that examination are discussed in "LITR Vertical In-Pile Loop" of this report.

Work also continued on the opening and sampling of MTR static corrosion capsules.[2] This work was facilitated by the modification of much of the experimental equipment in the cell.

Work has started on dismantling ANP in-pile loop 4 (ORNL-20-4). It is believed that the cell time required for the disassembly and analysis of this loop will be somewhat decreased by the use of improved tools and techniaues. These include small tools specially designed or modified to operate on the General Mills manipulator, such as shears, clamps, etc. A device to capture and retain fuel salt released during cutting operations has also been constructed and installed.

ANP in-pile loop 5 (ORNL-20-5), which could not be operated in the MTR because the loop could not be filled successfully, was sectioned and examined in the cells. The results of this examination have been reported.[3]

A great deal of supporting work for General Electric and other Solid State Division projects was also performed in the cells. This included dismantling of irradiation containers, removal of specimens, remote impact measurements, and various physical tests and measurements. In this connection a pinhole camera was successfully developed and operated by R. M. Carroll for autoradiographs of ceramic fuel element cores (discussed in "Autoradiography of Fuel Plates" of this report).

The Voland model 750-D analytical balance[4] was modified for density measurements and placed into operation in the cells. It was found to be quite satisfactory in all respects.

One of the Tell manipulators, used very little since the installation of the General Mills manipulators, was removed from the cell for a complete overhaul and modification of the electrical circuitry. It is felt that the Tell manipulator can still be quite useful after such modifications are made.

A concrete pad has been constructed north of Building 3025 for the storage of lead shipping containers, transfer casks, and other heavy equipment, thereby alleviating some of the congestion in the hot-cell loading area.

Initial layout drawings and design criteria are being formulated for a proposed hot-cell facility at the Laboratory, but no definite plans have yet been made.

Cell-use data for the first six months of 1956 exhibited no appreciable change from those for 1955,[4] with actual experimental operation accounting for 25% of the total cell time available and other associated operations requiring the remaining 75%.

The previously reported[4] effort to lower the radiation exposures to Hot Lab Section personnel has continued. At the current rate the average weekly dosage received per man during 1956 should be considerably less than that received during 1955, which was well below accepted ORNL tolerances.

---

[1] W. R. Willis *et al.*, *Solid State Semiann. Prog. Rep. Feb. 29, 1956*, ORNL-2052, p 24.

[2] W. E. Browning and H. L. Hemphill, *Solid State Semiann. Prog. Rep. Feb. 29, 1956*, ORNL-2052, p 20.

[3] C. Ellis *et al.*, *Examination of ANP In-Pile Loop 5*, ORNL CF-56-7-48 (July 16, 1956).

[4] S. E. Dismuke, M. J. Feldman, and E. S. Schwartz, *Solid State Semiann. Prog. Rep. Feb. 29, 1956*, ORNL-2052, p 40.

RADIATION METALLURGY

J. C. Wilson

CREEP AND STRESS-CORROSION TESTS OF INCONEL

W. W. Davis J. C. Zukas
N. E. Hinkle J. C. Wilson

A series of tube-burst tests on Inconel tubing at a stress of 2000 psi in helium at 1450 to 1500°F has been essentially completed on the bench and in the LITR. Insufficient data and scatter at 1450 and 1550°F prevented any quantitative interpretations at those temperatures. At 1500°F, however, ten tests were completed, and two more are under way. Specimens irradiated in HB-3 of the LITR broke at times varying from 113 to 560 hr; the arithmetic mean time for rupture was 260 hr. The bench-test specimens fractured at times varying from 350 to 1270 hr (with two specimens still in test at 407 and 490 hr), with a mean rupture time of at least 760 hr. Thus a decrease in rupture life of thin-walled tubes appears to have resulted from irradiation.

As was reported earlier,[1] the tubing stock used gave many indications of defects during nondestructive testing, but attempts to find the indicated defects metallographically were seldom successful. The presence of defects in the tubing may have influenced the radiation data. The rupture time obtained in a single test in argon by the Metallurgy Division[2] is about twice as high as the rupture times given above for the same stress. Extrapolation of the Metallurgy Division data at higher stresses shows a spread of about 2:1 in rupture times at 1500°F and 2000 psi. The data reported here showed spreads of about 4:1 in rupture time. The spread could be attributed to the presence of defects or differences in the structure of the material.

Carefully inspected tubing of the type to be used in the ART NaK-to-air radiators has been received for tube-burst tests in helium and in fused salt fuel mixtures. Added temperature controllers and pneumatic gaging equipment have been received with which to expedite the tests.

Another in-pile test (HB-3 of LITR) of the stress-corrosion rig was operated with fused salt fuel mixture No. 46 containing 25 mole % UF_4. Bench tests, improved heater design, and a reduction in the number of fins permitted the previous maximum operating temperature of 1200°F to be extended to 1500°F. Improved instrumentation has been built to reduce fission gas hazard and to record continuously all test variables. Work continues on improved safety systems for the high-pressure circuit to assure approval by MTR. Furnace arrangements for the MTR irradiations are also being tested, and modifications of an existing plug design are under way.

Two bench tests duplicating the tensile-creep test in HB-3 of the MTR were operated at 1500°F and a stress of 1500 psi in helium. Both bench specimens fractured out of gage at 542 and 614 hr, and the elongations were 1.0 and 1.9%, respectively. Preliminary examination suggested that local overheating outside the gage length had caused premature fracture. The in-pile test showed 1.7% elongation after 760 hr.

MTR STRESS-CORROSION APPARATUS

C. D. Baumann W. E. Brundage

Final assembly of the equipment for the stress-corrosion experiment has been held up by a delay in shipment of the proper high-temperature, high-pressure hermetic seals. The fused salt fuel mixture has been received and loaded in the specimen tube. Molybdenum wire heaters for the apparatus have been successfully fabricated inside a tubular ceramic form.

IRRADIATION OF SHIELDING MATERIALS

W. E. Brundage W. W. Davis J. C. Wilson

Testing equipment for the irradiation of a 1 wt % boron–stainless steel alloy is nearly completed and calibrated. Creep of the specimens under compression loading will be measured during the tests by a Bourdon-tube deflectometer. Pressurizing a bellows and lever arm system will impose a compressive stress on the specimen.

Short-time compression tests on copper–boron carbide cylinders were run at elevated temperatures for the Metallurgy Division. A special setup in an Instron testing machine permitted load-

[1] W. W. Davis *et al.*, *Solid State Semiann. Prog. Rep. Feb. 29, 1956*, ORNL-2052, p 5.

[2] J. W. Weir, *Met. Semiann. Prog. Rep. Oct. 10, 1955*, ORNL-1988, p 36.

deformation curves to be recorded directly. Yield stresses were determined for copper and copper plus 20 and 40 wt % B_4C at 1300°F. Creep tests were run at the same temperature at a stress of 500 psi. Unloading and reloading of short-time compression or creep specimens have improved resistance to deformation. This suggests that hot-pressing or hot-working improves the strength of the materials. Creep tests were also run at 1450 and 1500°F at a stress of 50 psi.

ENGINEERING PROPERTIES

O. Sisman

HIGH-TEMPERATURE CERAMIC FUELS

J. G. Morgan M. T. Morgan
R. M. Carroll P. E. Reagan

Fuel Irradiations

Four SiC-Si-UO_2 fuel plates, previously described,[1] have been exposed in the LITR at temperatures up to 1740° F. These fuel elements were fabricated[2] by the Ceramic Laboratory, Metallurgy Division, as follows:

1. The body components were mixed without fuel and put through a 12-mesh sieve. The composition of the body was 100 g of SiC, −1000 mesh, with an average particle size of ~10 μ; 3 g of Bakelite resin in powder form; 15 cc of pine oil.
2. A measured amount of the unfueled mixture was placed in a steel die $\frac{3}{4} \times 1\frac{3}{4}$ in. and leveled off, forming the bottom layer of the plate; 0.2 g of UO_2 was placed in a monolayer on the bottom layer. A mask was used to center the UO_2 so that there would be $\frac{1}{16}$-in. clearance on all sides, taking into consideration the final machined dimensions. The fuel was then covered by a top layer of unfueled mixture and a plate formed by pressing at 200 psi. The pressed plate was approximately $\frac{3}{16}$ in. thick.
3. The plate was covered with lampblack and heated to 200° C, driving off the pine oil and "setting" the binder.
4. The plate was then dipped in molten silicon at 1800° C, the volatiles from the resin binder being driven off as the plate entered the crucible. The silicon was soaked up in wicklike fashion by the porous SiC structure, forming a body of SiC in a silicon matrix.
5. The piece was machined to the final dimensions of $\frac{1}{2} \times 1\frac{1}{2} \times \frac{1}{8}$ in. and x-rayed to check for flaws and placement of fuel. The fuel plate composition was 0.2 g of UO_2 per plate, −70 +100 mesh, with an average particle size of 149 to 210 μ.

The appearance of typical specimens irradiated and unirradiated is compared in Fig. 27. The light-colored lines on the irradiated fuel plate are not cracks but regions of pure silicon resulting from the method of fabrication. The bulk properties of the fuel plates were not adversely affected under these irradiations.

Four ThO_2-UO_2 fuel rods have been irradiated[1] in the LITR at temperatures up to 1840° F. These bodies were fabricated by the ORNL Ceramic Laboratory as follows:[3] Steam-oxidized UO_2 was thoroughly mixed with precalcined ThO_2 containing $\frac{1}{2}$ wt % CaO; 1 wt % Carbowax 4000 was added as a binder, and the mixture was pressed into the desired shapes at 8000 psi. The pieces were fired in a helium atmosphere to 1750° C and then machined to the final size.

A comparison of the appearance of typical specimens irradiated and unirradiated is shown in Fig. 28. The bulk properties of the fuel material were not adversely affected under these irradiations.

A summary of the results of the postirradiation examinations is given in Table 4. Density changes under irradiation fell within the experimental error limit of ±0.2%. The samples were self-heated by fission, and the temperature cycles were caused by the reactor power cycles. The maximum heating or cooling rate experienced by the fuel elements was of the order of 200° C per minute.

Autoradiography of Fuel Plates

A pinhole camera was developed for taking autoradiographs of the ceramic fuel elements after reactor irradiation. Pictures obtained by this method show the location of the core fission products in relation to the clad material. While the radiation emitted from the core is primarily due to fission products, it was assumed that the disposition of the fission fragments corresponds to that of the uranium oxide. This assumption was strengthened when it was observed that the areas of greater density of fuel, as revealed by the radiograph, corresponded to areas of greatest radiation intensity. The unchanged proportions of the core indicated both that the clad is successful in retaining the great majority of the solid fission products and that the uranium oxide does not

[1] J. G. Morgan, R. M. Carroll, and M. T. Morgan, *Solid State Semiann. Prog. Rep. Feb. 29, 1956*, ORNL-2052, p 11.

[2] J. R. Johnson *et al.*, *High-temperature Ceramic Power Reactors Using SiC-Si Fuel Elements*, p 111, TID-2022 (June 1956).

[3] L. M. Doney, private communication.

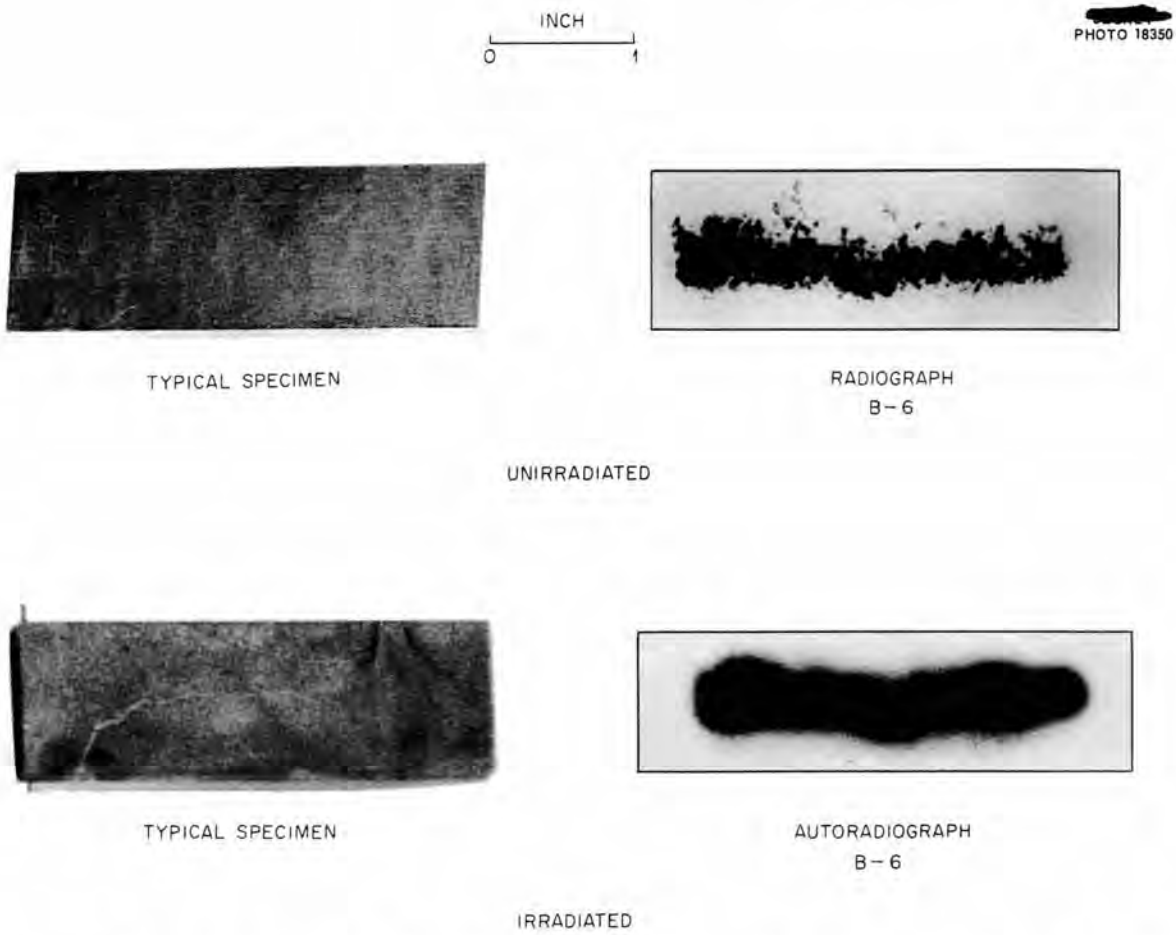

Fig. 27. Comparisons of SiC-Si-UO_2 Fuel Element Before and After Irradiation and of Pictures Obtained by X-Ray Photography with Autoradiographs Obtained by Pinhole Camera.

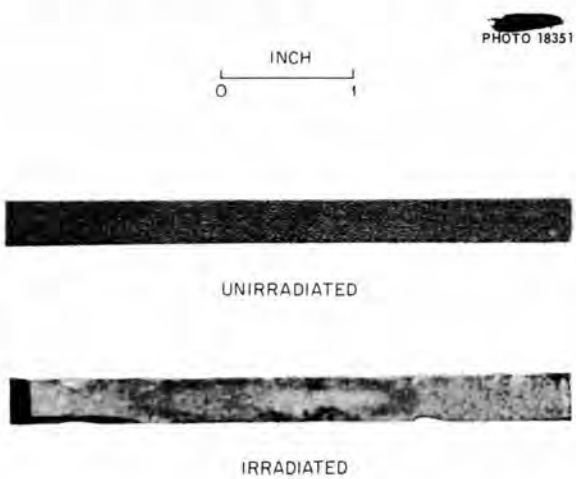

Fig. 28. Comparison of ThO_2-UO_2 Fuel Rods Before and After Irradiation.

migrate to any appreciable extent at the temperatures involved.

Previous work indicated that contact autoradiographs resulted in poor resolution compared with the results obtained with the pinhole camera. Figure 29 shows the pinhole camera which was designed for use in the Solid State hot cells. Any gamma radiation that is not converging to a point at the position of the pinhole is absorbed in the lead. A platinum insert containing the pinhole provides maximum gamma-ray shielding at this critical region. The optimum aperture size[4] is given by:

$$A_o = 2\sqrt{\frac{0.9\lambda\mu v}{\mu + v}} \quad ,$$

[4] J. E. Mack, *The Photographic Process*, McGraw-Hill, New York, 1939.

[redacted]

TABLE 4. RESULTS OF POSTIRRADIATION EXAMINATIONS OF SiC-Si-UO_2 FUEL PLATES AND ThO_2-UO_2 FUEL RODS

Sample No.	Material[a]	Thermal-Neutron Dosage (nvt)	Average Temperature (°F)	Hours at Temperature	Thermal Cycles[b]	Density (g/cc)	Dimensional Change After Irradiation[c] (in./in.)
A-2	SiC-Si-UO_2	2.4×10^{17}	1740	3	1	2.840	0 ± 0.0007
A-3	SiC-Si-UO_2	3.5×10^{19}	1475	533	9	2.835	0 ± 0.0007
B-6	SiC-Si-UO_2	4.3×10^{18}	1645	418	19	2.833	0 ± 0.0007
5	ThO_2-UO_2	5×10^{19}	1385	557	13	9.135	0 ± 0.001
6	ThO_2-UO_2	5×10^{19}	1385	557	13	9.118	0 ± 0.0008
1	ThO_2-UO_2	1×10^{20}	1840 1475	780 400	33 20	8.929	0 ± 0.0008
3	ThO_2-UO_2	1×10^{20}	1840 1475	780 400	33 20	9.087	Sample broken in handling

[a]SiC-Si-UO_2 material contained 4 wt % uranium enriched 94%; ThO_2-UO_2 material contained 2.5 wt % uranium enriched 94%.

[b]Each cycle was from reactor water temperature to full operating temperature and return.

[c]Maximum deviation includes irregularities in the samples.

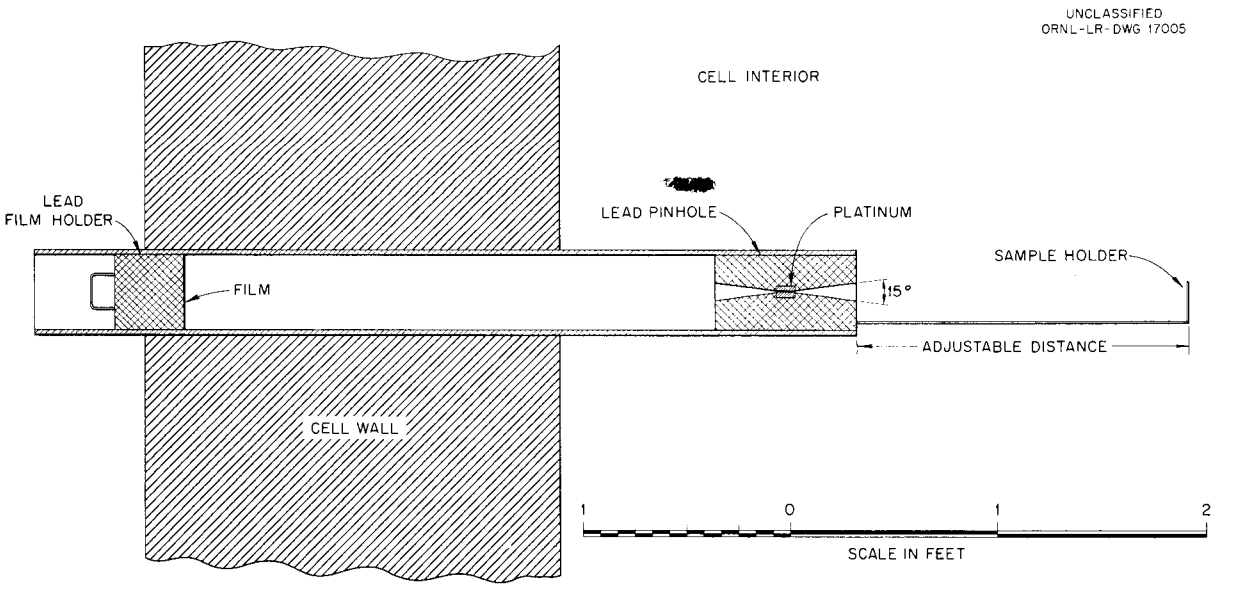

Fig. 29. Schematic Drawing of Pinhole Autoradiograph Camera.

where

A_o = optimum aperture diameter,

λ = wavelength of radiation,

μ = distance of object from aperture,

v = distance of image from aperture.

The camera was constructed with a 15-deg-angle cone cut from lead, approximated by concentric drilled holes, and terminating in a 0.0125-in.-dia pinhole. Eastman Kodak medical x-ray film, no-screen, was mounted in the shielded film holder and the sample was suspended in front of the pinhole at the other end of the camera.

Before irradiation the position of the UO_2 within the element was determined by x-ray photography, which revealed the individual grains of uranium oxide. In Fig. 27 x-ray pictures are compared with a picture taken with the pinhole camera. While the autoradiograph does not possess as high a resolution as the x ray, nevertheless, it clearly follows the irregularities of the original core. Other investigators[5] have observed that UO_2 diffuses in some ceramics at elevated temperatures. This would invalidate the clad protection of this type of element. There appears to be little or no diffusion of UO_2 in the SiC-Si as a result of these irradiations.

Fission-Gas Release

A test was conducted to identify fission gases released by irradiated ThO_2-UO_2 samples Nos. 1 and 3 (see Table 4) and to determine the quantity of these gases. Since the material is not clad, fuel is exposed at all surfaces. The samples were irradiated in a capsule designed with the gas-sampling feature shown in Fig. 30. This feature consists of a short section of $\frac{3}{8}$-in. tubing, A, welded on the bottom of the capsule. The end of this tube is weld-sealed with a plate 0.019 in. thick for piercing. The sampler receives the capsule tube and is sealed to the capsule by a standard $\frac{3}{8}$-in. Swagelok fitting, B. A sharp-pointed hypodermic plunger is forced upward and through the end plate by turning the nut, C. A valved receiver, D, previously evacuated, is attached to the sampler by an O-ring seal. This container receives the gas when the capsule is pierced and the receiver valve is opened. A liquid air bath may be applied to the receiver by elevating the bath on the platform, E. Portions of the gas are transferred from the valved receiver to aluminum

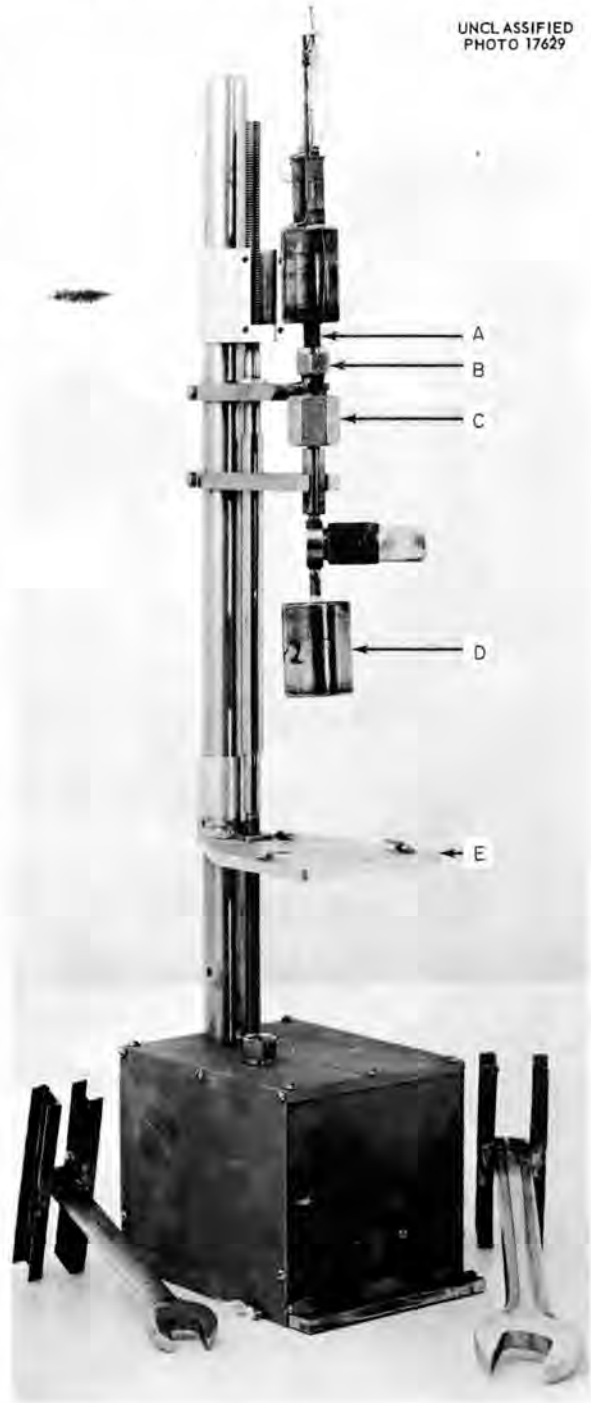

Fig. 30. Container with Gas-Sampling Feature.

[5] J. F. Quirk *et al.*, *Uranium Migration in UO_2-Bearing Ceramics*, TID-10045.

counting cans in sufficiently small quantities to allow handling outside the hot cell. Radioactive argon was used for calibrating the sampling procedure so that the activity data could be extrapolated back in terms of total activity of gas in the original sample container.

Gamma-ray spectrometer curves were recorded at three- to five-day intervals on the counting can, which contained 5% of the gas volume in the irradiated capsule. The only significant peak appeared at 0.081 Mev, which is the gamma energy of Xe^{133}. The decay of the amplitude of this peak is shown in Fig. 31.

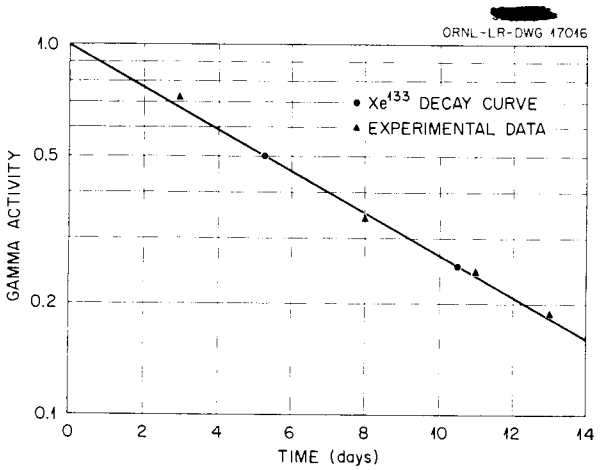

Fig. 31. Decay Curve of Xe^{135}.

The activity of 5% of the gas in the irradiated capsule was measured 22 days after reactor shutdown. At 1 photon/d this fraction showed an activity of 8.7×10^5 d/sec, which corresponds to 1.7×10^7 d/sec in the total gas volume in the capsule. The Xe^{133} activity released from the two samples is then 3.14×10^8 d/sec at the end of the irradiation period; 99.8% of the total Xe^{133} produced remained in the samples. Based on the assumption that there was uniform production of fission products throughout the sample, the maximum depth from which the Xe^{133} escaped is 5×10^{-5} in.

REACTOR SHIELD MATERIALS

J. G. Morgan M. T. Morgan
P. E. Reagan R. M. Carroll

For ART application a desirable thermal-neutron shield should have a high absorption cross section, be compatible with adjacent reactor materials, be able to withstand elevated temperatures, and retain its bulk structure under irradiation. Gas release from the material should be at a minimum. For use at temperatures up to 1600° F, clad cermets are one of the groups of materials of interest.

Two cermet shield materials (prepared by the Metallurgy Division) are CaB_6-Fe and BN-Ni, both clad with type 304 stainless steel. The cermets were fabricated as follows:[6]

1. The powders were mixed for 2 hr in an offset rotary blender.
2. The mixed powders were cold-pressed at 33 tsi in a $2 \times 2\frac{1}{4}$ in. steel die.
3. The cold-pressed compacts were sintered for 1 hr at 2000° F in a hydrogen atmosphere.
4. The sintered compacts were coined at 33 tsi to 0.250 in. thickness in a $2 \times 2\frac{1}{4}$ in. steel die.
5. The cermet cores were encapsulated in type 304 stainless steel picture frames.
6. The picture frames were hot-rolled at 2000° F to a total reduction in thickness of 7:1.
7. The specimens were machined from rolled composite sheet.

The specimens were $0.1875 \times 0.500 \times 0.050$ in. thick; the powder particle sizes and compositions of the cermet core materials are given in Table 5.

A CaB_6-Fe sample was irradiated in helium in the LITR to a thermal-neutron dosage of 5.2×10^{19} *nvt*. The sample, sealed in quartz, was cooled by the LITR water. Metallographic examination[7] after irradiation (Fig. 32) showed that the clad-core interface had retained its continuity. The core material was clad to ensure its compatibility with the Inconel to be used as the structural material in a reactor. Many of the CaB_6 crystals are observed in the core matrix, although some have been removed in sample preparation. The samples shown in Fig. 32 are shown again in Fig. 33 at a lower magnification so that the cladding on both faces of the sample can be seen. There is no evidence of gross cracking in the core or of deformation of the sample. Because of the inhomogeneity of the core, hardness tests were inconclusive; however, a slight increase in hardness was observed.

Samples of BN-Ni are being irradiated in the LITR for six weeks and will be examined after

[6] J. H. Coobs, private communication.
[7] A. E. Richt, private communication.

TABLE 5. PARTICLE SIZES AND COMPOSITIONS OF CERMET SHIELD MATERIALS

Cermet	Component	Particle Size (μ)	Weight of Component (%)	Volume of Component (%)
CaB_6-Fe	CaB_6	44 to 100	7.6	21.0
	Fe	147	92.4	79.0
BN-Ni	BN	10	10.3	30
	Ni	10	89.7	70

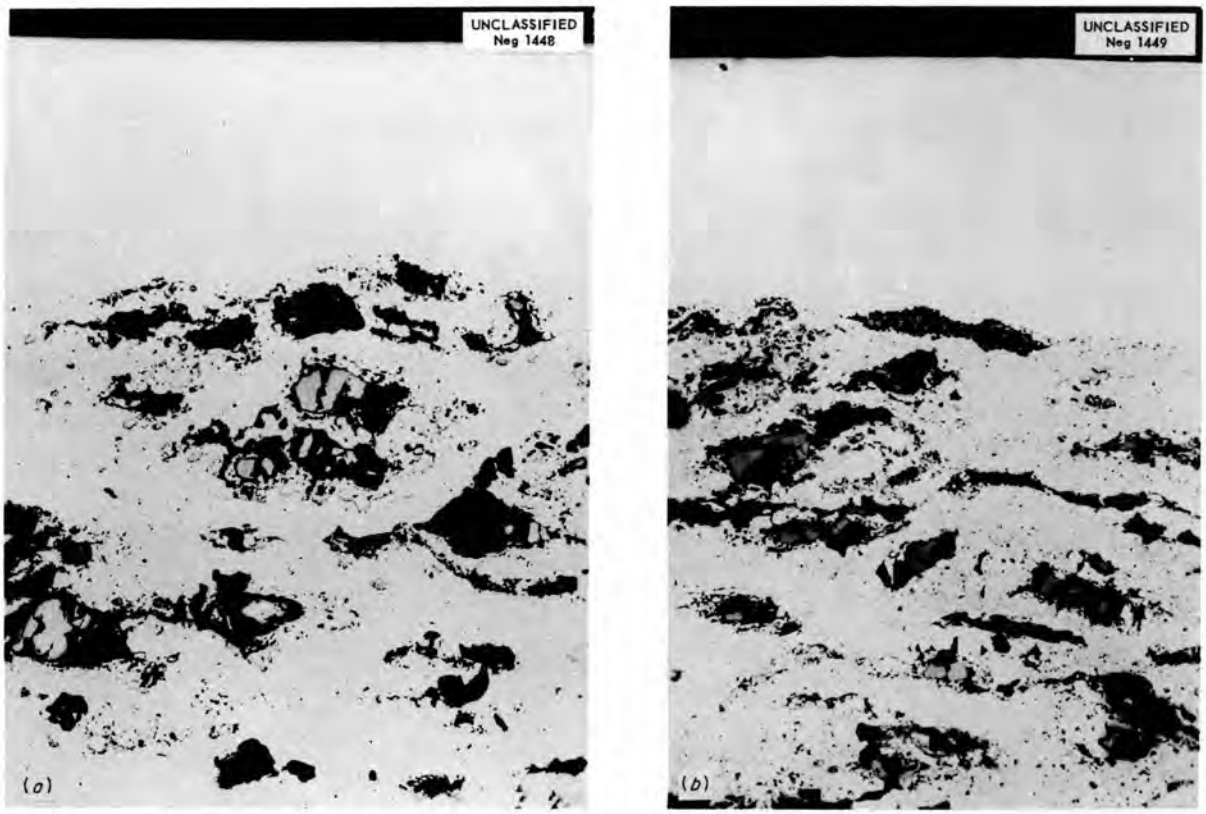

Fig. 32. Type 304 Stainless-Steel-Clad CaB_6-Fe Cermet Before and After Irradiation in the LITR to a Thermal-Neutron Dose of 5.2×10^{19} *nvt*. (*a*) Unirradiated. (*b*) Irradiated. 250X. Reduced 27%.

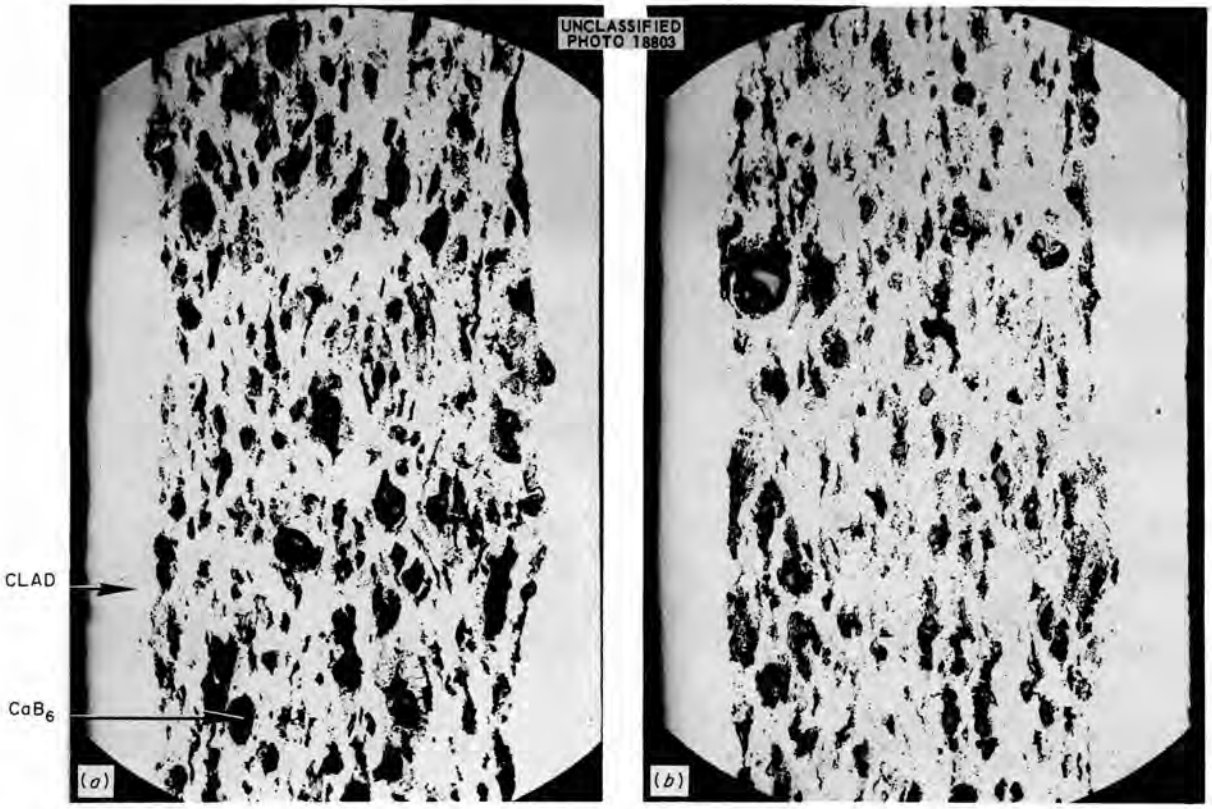

Fig. 33. Type 304 Stainless-Steel-Clad CaB_6-Fe Cermet Specimens Shown in Fig. 32 at a Lower Magnification. Both cladding-cermet interfaces can be seen. (*a*) Unirradiated. (*b*) Irradiated. 75X. Reduced 27%.

another three weeks of exposure. The specimens are being irradiated in the same facility as used for the above test. In addition, the clad BN-Ni material is being given a high-temperature irradiation in C-48 of the LITR. The sample was sealed under vacuum in an Inconel capsule. A platinum resistant heater is being used to control the temperature during irradiation at 1600° F. Gas formed as a result of the irradiation will be removed and analyzed.

Boron Carbide

The cursory radiation evaluation tests were completed on B_4C for use as a neutron shield material. Twenty samples, including six different fabrication specifications, were irradiated in the LITR to an average thermal-neutron dosage of 6×10^{19} *nvt*. The samples, $\frac{1}{4} \times \frac{1}{4} \times \frac{1}{2}$ in., were sealed in a helium atmosphere and cooled by the reactor water.

Fabricational data of the six B_4C bodies are listed below:

Sample A-N

Hot-pressed and sintered

High density

Boron analysis, 65.9 wt %

Hard and impervious

Sample B-N

Hot-pressed and fired at above 2000° C

Fabricated from high-purity boron carbide, 35-mesh and finer

Boron analysis, 71.8 ± 0.4 wt %

Hard, strong, and impervious

Sample C-N

Hot-pressed and fired at above 2000° C

Fabricated from 60-mesh, and finer, technical-grade boron carbide

Boron analysis, 62.4 ± 0.4 wt %

Hard, strong, and nearly impervious

Sample A-C

Cast and sintered and then bonded with SiC

Porous and friable

Sample B-C

Cast, then fired at 1350° C and refired at 2000° C

Fabricated from basic mixture of 90% B_4C grain and 10% 20-mesh silicon metal

Porous and friable

Boron analysis, 64.7 ± 0.5 wt %

Sample C-C

Cast, then fired at 1350° C and refired at 2000° C

Fabricated from basic mixture of 80% B_4C, 10% 200-mesh, and finer, boron metal powder, and 10% 200-mesh, and finer, silicon metal powder

Porous and friable

Boron analysis, 67.8 ± 0.4 wt %

The trace impurities determined by spectrographic analysis are listed in Table 6. The results of the tests are given in Table 7.

X-ray examination of irradiated specimen A-C showed an increase in disordering and the subsequent appearance of a lessening of the degree of x-ray crystallinity. No particle-size broadening was indicated.[8]

MTR Irradiations

Six samples of copper–boron carbide were prepared for irradiation and shipped to the MTR. The capsules will be inserted in an "A" piece and irradiated to a thermal-neutron dosage of 3×10^{20} *nvt*. The samples will be irradiated at 1600° F. The instrumentation for the experiment has been constructed and shipped to the site. The test will be operated to attain a maximum boron burnup equivalent to that expected in the ART.[9] The samples[10] are 0.1875 × 0.500 × 0.102 in. thick and are clad on two faces. The composition is 6.6 wt % B_4C, –325 mesh, clad with a 3-mil copper barrier over which is clad 7 mils of type 430 stainless steel. The samples are mounted in two capsules, three samples per capsule.

[8] G. E. Klein, private communication.

[9] A. M. Perry, private communication.

[10] M. R. D'Amore, private communication.

TABLE 6. SPECTROGRAPHIC ANALYSIS OF B_4C SAMPLES

Impurity	Limit of Detection* (%)	Amount of Impurity (%)					
		Sample A-N	Sample B-N	Sample C-N	Sample A-C	Sample B-C	Sample C-C
Al		0.01–0.1	1–10	0.1–1	0.1–1	0.1–1	0.1–1
Ca		0.001–0.01	0.01–0.1	0.001–0.01	0.001–0.01	0.001–0.01	0.001–0.01
Cr	0.004	*	*	*	0.01–0.1	0.01–0.1	0.01–0.1
Cu	0.0001	*	0.01–0.1	*	*	*	*
Fe		0.01–0.1	0.1–1	0.1–1	1–10	0.1–1	1–10
Mg		0.0001–0.001	0.001–0.01	0.0001–0.001	0.001–0.01	0.001–0.01	0.001–0.01
Mn	0.001	*	0.01–0.1	*	0.01–0.1	0.01–0.1	0.01–0.1
Ni	0.02	*	*	*	0.1–1	0.01–0.1	0.01–0.1
Ti	0.04	*	0.1–1	0.1–1	0.1–1	0.1–1	0.1–1
Zr	0.03	*	0.1–1	0.1–1	1–10	1–10	1–10

*Element sought but not found.

Figure 34 shows the three samples mounted in a support grid with the two thermocouples, for monitoring the sample temperature, and a cobalt foil flux monitor included. As shown in Fig. 35, the support grid assembly is weld-sealed in a helium atmosphere in an inner capsule; an electrical heater made of platinum coils in an alumina form is inserted in a stainless steel can, B; thermocouple leads are brought out of the inner capsule, C, through a hermetic ceramic seal, and the wires

TABLE 7. RESULTS OF IRRADIATING BORON CARBIDE SAMPLES IN THE LITR TO AN AVERAGE THERMAL-NEUTRON DOSAGE OF 6×10^{19} *nvt*

Specimen	Gas Evolution (cc)	Density Change (g/cc)	Dimensional Change (in./in.)
A-N Three samples ρ = 2.49 g/cc	0 ± 0.1	0 ± 0.01	0 ± 0.001
B-N Three samples ρ = 2.17 g/cc	0 ± 0.1	0 ± 0.05	0 ± 0.001
C-N* Three samples ρ = 2.02 g/cc	0 ± 0.1	0 ± 0.1	0 ± 0.001
A-C** Three samples	8.1 cc/g (av)		
B-C Six samples	0 ± 0.1	Samples too porous and friable to allow precise density or dimensional measurements	
C-C Six samples	0 ± 0.1		

*Bulk density; sample slightly porous.
**Black deposit on container.

UNCLASSIFIED
PHOTO 18123

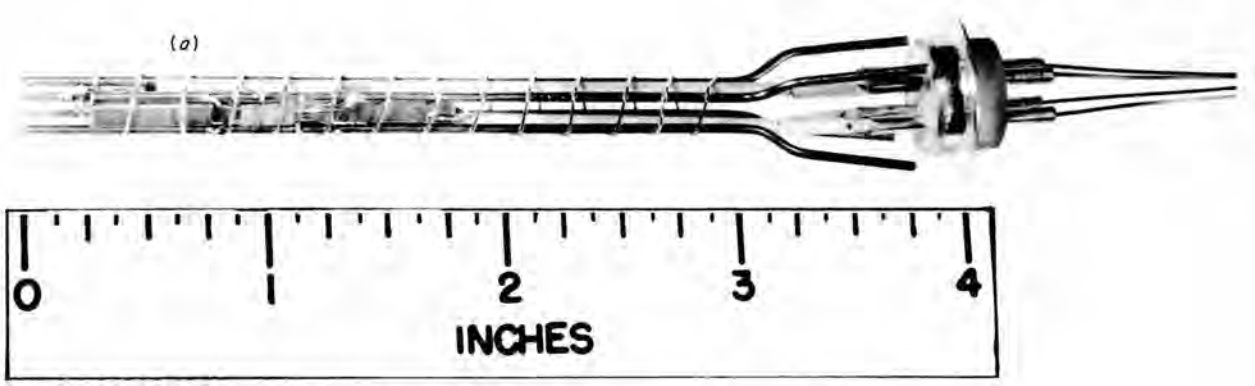

Fig. 34. Clad Cermet Sample Assembly.

UNCLASSIFIED
PHOTO 18124

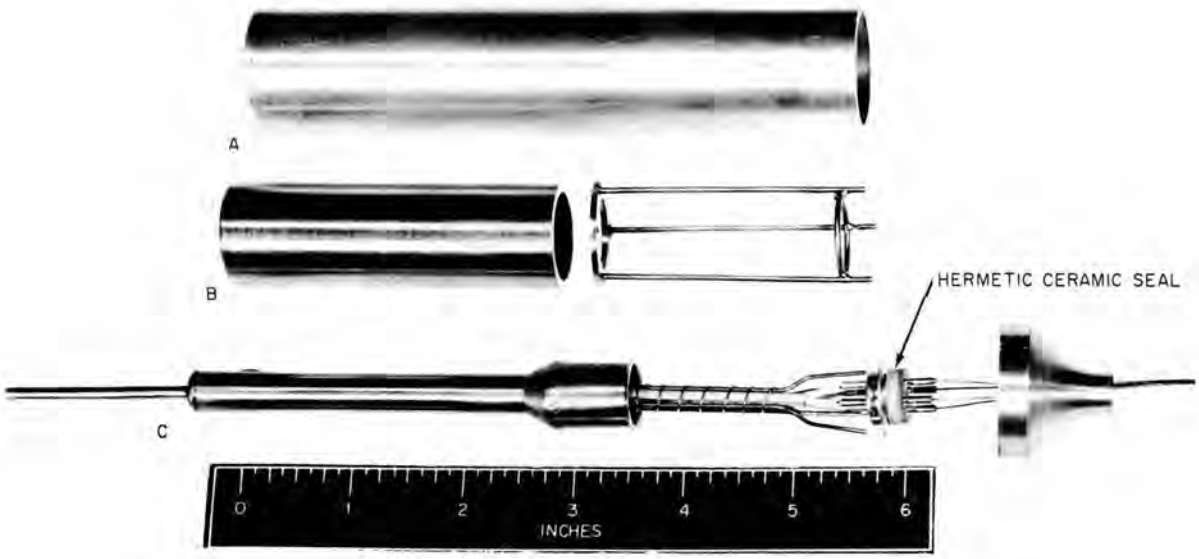

Fig. 35. Components of Assembly Shown in Fig. 34.

lead out through a small aluminum tube to the top of the reactor. The assembly is welded into an aluminum container, A. After irradiation, the samples will be returned to ORNL for postirradiation examination.

Boron Nitride

Another promising neutron shield material is hot-pressed boron nitride. Boron contents of up to 44 wt % can be obtained with a density of 2.1 g/cc in a molded and self-bonded structure. Boron nitride has a crystalline structure similar to graphite, and directionalism is present in all physical properties,[11] especially thermal expansion. Pure (98% and above) boron nitride powder was obtained from two sources and complete analysis determined. Bodies from these powders will be fabricated at the laboratory, and irradiation studies will then be undertaken.

[11] K. M. Taylor, *Ind. Eng. Chem.* **47**(12), 2506 (1955).